Diabetologia
https://doi.org/10.1007/s00125-026-06906-z

EXTENDED ARTICLE

Pregestational maternal diabetes primes neonatal beta cell dysfunction with structural remodelling, impaired calcium buffering and altered mTORC2–Gαq–PKCα signalling in a pig model

Libera Valla[1,2] · Minas F. Schwager[3,4] · Christian M. Cohrs[5,6,7] · Jan B. Stoeckl[8] · Christos Karampelias[3,5] · Bachuki Shashikadze[8] · Birgit Rathkolb[1,5,9] · Richard Lindner[1,2] · Martin Kraetzl[1,2] · Simone Renner[1,2,5,10] · Mireia Molina van den Bosch[3] · Kaiyuan Yang[3] · Michael Sterr[3,5] · Anika Böttcher[3,5] · Martin Hrabě de Angelis[5,9,11] · Stephan Speier[5,6,7] · Thomas Fröhlich[8] · Fabian J. Theis[4] · Heiko Lickert[3,5] · Eckhard Wolf[1,2,5,8,10] · Elisabeth Kemter[1,2,5,10]

Received: 24 February 2026 / Accepted: 14 August 2026
© The Author(s) 2026

Abstract

Aims/hypothesis Offspring of mothers with diabetes are at increased risk of developing type 2 diabetes, and this predisposition is established during fetal life. The aim of this study was to define the functional, morphological and molecular alterations in neonatal pancreatic islets associated with maternal hyperglycaemia, with a particular focus on beta cells, an area that remains poorly understood. Given its similarity to humans in endocrine pancreas development, the pig was used as a translational animal model.

Methods Using genetically diabetic and beta cell reporter pig models, we performed functional assessments of glucose-stimulated insulin secretion in vivo and in situ using fresh pancreatic tissue slices from neonatal piglets born to hyperglycaemic mothers (PHGs) or normoglycaemic mothers (PNGs). Morphological and molecular profiling, including proteomics and single-cell RNA-seq, were performed to elucidate molecular changes reflecting the developmental impact of maternal diabetes on offspring metabolic health, with a particular focus on neonatal beta cells.

Results PHGs were born hyperglycaemic, hyperinsulinaemic and insulin resistant, exhibiting markedly delayed glucose and insulin response curves following oral glucose administration, with more pronounced effects in male piglets. Elevated basal insulin secretion and an almost blunted glucose responsiveness of pancreatic tissue slices were associated with increased insulin and somatostatin content, expansion of beta (+35%) and delta (+47%) cell populations, and organisation into larger islet clusters. Neonatal PHG islets exhibited a molecular profile consistent with intrinsic beta cell dysfunction that partially overlapped with type 2 diabetes (e.g. RBP4 upregulation), together with alterations in glucose sensing (near absence of GLUT2), nutrient metabolism resembling congenital hyperinsulinism (*HADH* downregulation), and cytosolic Ca^{2+} homeostasis (near absence of the Ca^{2+} buffer calbindin D28K). In addition to an ATF4-dominated stress signature, a shift towards a distinct PHG beta cell subcluster characterised by low expression of ribosomal genes was observed, with an adaptive early-response-gene-mediated transcriptional reactivity. In contrast to the Gαs–adenylyl cyclase–cAMP–PKA signalling axis that dominated in PNG beta cells, neonatal PHG beta cells displayed distinct alterations in Gαq–PLC–PKCα signalling components, the mTORC2 target PKCα, and CREB1, suggesting a restructured signalling architecture.

Conclusions/interpretation Our findings reveal altered islet modelling with a unique beta cell dysfunction profile that partially overlaps with, but differs from, that of type 2 diabetes. A shift towards a beta cell subcluster exhibiting an adaptive early-response-gene-mediated transcriptional reactivity and an ATF4-associated transcriptional stress signature provides insight into molecular alterations associated with fetal exposure to maternal diabetes and may contribute to the increased risk of metabolic disease in offspring.

Keywords Beta cell stress adaptation · Developmental programming · Islet cell plasticity · Maternal hyperglycaemia · mTOR signalling · Neonatal hyperinsulinaemia · Neonatal insulin resistance · Pancreatic beta cell dysfunction

Libera Valla and Minas F. Schwager contributed equally.

Extended author information available on the last page of the article

Published online: 06 November 2026

Research in context

What is already known about this subject?

- Offspring of mothers with diabetes are born with hyperglycaemia and hyperinsulinaemia, which normalise postnatally
- The offspring's increased risk of type 2 diabetes later in life is associated with epigenetic changes in cord blood cells

What is the key question?

- What is the neonatal beta cell profile and function associated with maternal hyperglycaemia?

What are the new findings?

- Contrary to the prevailing hypothesis of accelerated islet maturation, endocrine cells in the neonatal pancreas of offspring of hyperglycaemic mothers exhibited dysfunction with altered structural and signalling architecture, likely as a compensatory response to increased metabolic demands in a chronically hyperglycaemic, meta-inflammatory developmental environment
- Basal insulin hypersecretion and glucose unresponsiveness in beta cells from neonates of hyperglycaemic mothers were associated with a molecular dysfunction profile that only partially overlapped with type 2 diabetes and exhibited distinct features, including an ATF4-dominated stress signature and widespread early-response transcript signature
- A restructured signalling architecture was present with concomitant involvement of mTORC2, Gαq-PLC-PKCα and CREB1 signalling

How might this impact on clinical practice in the foreseeable future?

- This knowledge may help identify key targets for preventing individuals exposed to maternal diabetes from developing type 2 diabetes later in life

Abbreviations

$beta^{rp\text{-}high}$	Beta cells with high ribosomal gene transcript content
$beta^{rp\text{-}low}$	Beta cells with low ribosomal gene transcript content
CREB	cAMP-responsive element binding protein
DAG	Diacylglycerol
DEGs	Differentially expressed genes
DI	Disposition index
DIA	Data-independent acquisition
eGFP	Enhanced green fluorescent protein
GCG	Glucagon
GPCRs	G-protein-coupled receptors
GSIS	Glucose-stimulated insulin secretion
HVGs	Highly variable genes
ICC	Intraclass correlation coefficient
LSM	Least squares mean
MIDY	Mutant *INS* gene-induced diabetes of youth
mTOR	Mechanistic target of rapamycin
PHG	Piglet born to a hyperglycaemic mother
PKA	Protein kinase A
PKC	Protein kinase C
PNG	Piglet born to a normoglycaemic mother
PPY	Pancreatic polypeptide
QUICKI	Quantitative insulin sensitivity check index
scRNA-seq	Single-cell RNA-seq
SIDD	Severe insulin-deficient diabetes
SPINA	Structure parameter inference approach
SPINA-Gbeta	SPINA-secretory capacity of pancreatic beta cells
SPINA-GR	SPINA-estimated insulin receptor gain
SST	Somatostatin
SYP	Synaptophysin
TP	Time point
UMAP	Uniform Manifold Approximation and Projection
UPR	Unfolded protein response
WSI	Whole-slide images
WT	Wild-type

Introduction

Maternal diabetes not only affects the health of the pregnant woman but also may adversely influence the offspring's metabolic health through an altered intrauterine environment [1]. Studies, including the Hyperglycaemia and Adverse Pregnancy Outcomes Follow-up Study (HAPO-FUS), report increased risks of stillbirth, altered fetal growth and neonatal metabolic disturbances such as hyperinsulinism and insulin resistance in offspring of diabetic mothers [2, 3]. Maternal diabetes increases the risk of type 2 diabetes up to eightfold later in life in offspring [4].

The Pedersen hypothesis (1952) was one of the first to postulate a causal link between maternal hyperglycaemia and fetal hyperglycaemia and hyperinsulinaemia [5]. Later studies showed that elevated maternal insulin, triacylglycerols and NEFA also disrupt fetal metabolism and increase later metabolic disease risk in offspring [6, 7]. The association with offspring's increased risk of developing type 2 diabetes may arise from early-life priming of pancreatic beta cells, which are most plastic in humans until ~2–3 years of age [1, 8]. During this critical window, islet development is shaped by genetic and environmental factors, including maternal nutritional cues and stressors such as inflammation, hyperglycaemia and lipotoxicity [1, 9]. However, the molecular mechanisms underlying beta cell vulnerability, early exhaustion and failure in offspring of diabetic mothers, remain poorly understood as the direct effects of hyperglycaemia and hyperinsulinaemia on the endocrine pancreas cannot be studied in humans during this sensitive early postnatal period.

This study aimed to elucidate how maternal diabetes shapes offspring metabolic health, focusing on the functional and molecular alterations of neonatal beta cells. Given its close similarity to humans in endocrine cell differentiation and functional maturation during pancreas development [10], the pig was used as a translational animal model.

Methods

Animal model and management of maternal diabetes Two transgenic pig lines were used. The *INS*^{C94Y} pig line harbouring a mutant *INS* p.C94Y transgene, which leads to permanent neonatal diabetes, serves as a large-animal model for mutant *INS* gene-induced diabetes of youth (MIDY) [11]. The beta cell-specific expression of enhanced green fluorescent protein (eGFP) in *INS*-eGFP transgenic pigs allows beta cell sampling by flow cytometry [12]. To minimise variation in genetic background, the normoglycaemic and hyperglycaemic sows used in this study were full siblings generated by mating wild-type (WT) sows with either an *INS*^{C94Y}/*INS*-eGFP dual transgenic or an *INS*^{C94Y} transgenic boar. The resulting sows were mated with either one WT boar or one *INS*-eGFP transgenic boar.

Fasting blood glucose levels of diabetic breeding sows were maintained within the range of 5.6–8.3 mmol/l by daily insulin treatment before pregnancy and for the first 3 weeks after mating. After pregnancy confirmation (3 weeks after mating), daily insulin treatment was adjusted within 1 week to maintain a fasting blood glucose level around 16.7 mmol/l. Blood glucose concentrations were measured daily in fasted pigs. Diabetic pigs were treated with a combination of long-acting and short-acting insulin (Lantus and Novorapid) [11]. As we previously demonstrated, fasting blood glucose levels in pregnant WT sows were comparable with those in non-pregnant WT sows, except for a moderate increase during the last trimester that remained within the normoglycaemic range [13]. Therefore, blood glucose levels were not assessed in WT sows in the present study. A species comparison of developmental milestones, including gestational length, pancreatic islet development, the principal nutrient sources before and after birth, and the postnatal dynamics of beta cell proliferation and apoptosis, is shown in electronic supplementary material (ESM) Fig. 1.

All experiments were conducted in accordance with the German Animal Welfare Act, following the ARRIVE guidelines and Directive 2010/63/EU, and were approved by the local authority (Regierung von Oberbayern). Pigs (Landrace-Swabian-Hall background) were housed under designated pathogen-free conditions, had free access to water and were fed a commercial food. Piglets were housed in a farrowing pen together with their mother sow, and a heated nest was offered to the piglets. Piglets were suckled by their own mothers, whose milk composition was not evaluated.

Clinical analyses and OGTT of newborn piglets Starting on pregnancy day 113, pregnant sows were monitored for signs of birth. If birth did not occur spontaneously by embryonic age of 115 days (E115), it was hormonally induced. Shortly after birth, before the first milk intake, the first ten piglets born from each litter studied were separated from the mother, weighed and placed in a rescue deck under a red heating lamp. After a 30 min recovery period, an OGTT was performed by administering 4 ml of a 50% (wt/vol.) glucose solution (B. Braun, Melsungen, Germany) per kg body weight via a nasogastric tube. Blood glucose concentrations were measured before glucose administration (time point [TP] 0), and then at TP 15, 30, 45, 60, 90 and 120 min after glucose administration by ear vein puncture using a glucometer (FreeStyle-Freedom Lite, Abbott Diabetes Care, Alameda, CA, USA). EDTA blood was collected from the jugular vein at TP 0, 30, 60 and 120 min, immediately placed on wet ice, and centrifuged at 170 *g* for 20 min at 4°C. Plasma was aliquoted and stored at –80°C [14]. All

piglets born to hyperglycaemic mothers and harbouring the mutant *INS* p.C94Y transgene were excluded from all subsequent analyses.

Clinical-chemical analysis Clinical-chemical variables were determined from EDTA plasma using an AU480 auto analyser (Beckman-Coulter) and reagent kits from Beckman-Coulter, Randox or Wako Chemicals. Plasma insulin concentrations were measured in duplicates using an ultrasensitive insulin ELISA kit (10-1132-01, Mercodia, Uppsala, Sweden). In a recent study investigating liver multi-omics of the same cohort of animals through proteomic, metabolomic and lipidomic analyses [15], glucose and insulin concentrations on the day of birth were determined and used to calculate indices of insulin resistance.

The AUC for glucose and insulin concentrations during OGTT and glucose-stimulated insulin secretion (GSIS) was calculated using GraphPad Prism software (versions 5.02 and 10.1.2). If blood sampling from an animal failed at either TP 0 or TP 120, it was excluded from the AUC calculation. Various indices, commonly used as surrogate markers for insulin resistance, insulin sensitivity and beta cell function, were calculated from the glucose and insulin levels obtained during the OGTT. Insulinogenic index, disposition index (DI), and Matsuda index (also called ISIcomp) [16] were calculated using the support from https://mmatsuda.diabetes-smc.jp/MIndex.html. Quantitative insulin sensitivity check index (QUICKI) was calculated using the formula 1/(log[fasting insulin μU/ml] + log[fasting glucose mg/dl]) [17]. Structure parameter inference approach (SPINA)-secretory capacity of pancreatic beta cells (SPINA-Gbeta), which is a surrogate marker for beta cell function expressed as maximum amount of insulin that beta cells can produce per time unit, SPINA-estimated insulin receptor gain (SPINA-GR), which is a calculated marker for insulin sensitivity, and SPINA-DI, which marks loop gain of insulin–glucose homeostasis, were calculated according to Dietrich and coworkers using the R software package [18, 19].

Necropsy Necropsy was performed following exsanguination under pre-terminal ketamine-azaperone anaesthesia with fentanyl supplementation on non-fasted piglets born to hyperglycaemic mothers (PHGs) and piglets born to normoglycaemic mothers (PNGs) at postnatal days 1–4, as indicated. Organs were dissected and weighed to the nearest milligram. Tissue samples were collected as described previously [20] and routinely fixed in 4% PBS-buffered paraformaldehyde for 2 days, followed by paraffin embedding or frozen immediately on dry ice and stored at −80°C for molecular profiling. Additionally, serum, EDTA plasma, Li-heparin plasma and urine were collected, aliquoted and stored at −80°C.

In situ dynamic GSIS in pancreatic tissue slices Dynamic GSIS was assessed in situ in living porcine pancreatic tissue slices from non-fasted 2- to 4-day-old PHGs and PNGs, with a modified protocol adapted from Speier and colleagues [21]. Animals from different litters were used, and a maximum of two animals were processed per day due to the experimental workflow's capacity. Consequently, complete randomisation was not feasible, and allocation to experimental groups was constrained by the availability of animals with the required genotype, sex and predefined narrow age range. Immediately after euthanasia and exsanguination, 37°C warm 1.75% low-melting agarose (39346-81-1, Carl Roth) supplemented with 25 KIU/ml aprotinin (A2300-05, US Biological Life Science) was applied into the splenic pancreas lobe by exogenous G27 needle injection. After hardening of agarose, small pieces (1–1.5 mm^3) of the splenic lobe were cut and embedded in 2.5% low-melting agarose. Tissue slices were obtained using a semi-automated vibratome (Leica VT1200S) at a thickness of 150 μm, an amplitude of 1.0 and a feed of 0.1 mm/s. Following a 2 h equilibration period on an orbital shaker at room temperature in KRB (in mmol/l: 137 NaCl, 5.36 KCl, 0.34 Na_2HPO_4, 0.81 $MgSO_4$, 4.17 $NaHCO_3$, 1.26 $CaCl_2$, 0.44 KH_2PO_4, 10 HEPES, 0.1% BSA, pH 7.3) supplemented with 3 mmol/l glucose and aprotinin (25 KIU/ml), to establish a comparable fasted metabolic baseline across animals, two or three slices were placed each into a closed perifusion chamber (64-0223 and 64-0281 [P-5], Warner Instruments, Holliston, MA, USA) and connected to a perifusion system with automated tray handling (PERI4-02-230-FA, Biorep Technologies, Miami, FL, USA). Tissue slices were perfused at a flow rate of 100 μl/min and samples were collected into 96-well plates at 120 s intervals. Slices were flushed for 60 min with 3 mmol/l glucose KRB containing aprotinin (25 KIU/ml) to wash out accumulated hormones and enzymes from the tissue. Then, slices were perfused with KRB buffer containing 3 mmol/l glucose for 10 min, followed by 30 min in 16.7 mmol/l glucose, 30 min in 3 mmol/l glucose, 20 min in 16.7 mmol/l glucose plus 60 mmol/l KCl, and, finally, 10 min in 3 mmol/l glucose. All solutions were supplemented with aprotinin (25 KIU/ ml). After perifusion, tissue slices were gently transferred to a tube containing 500 μl acid ethanol. All samples were frozen at –20°C until assayed for insulin content using an ultrasensitive insulin HTRF assay (62IN2PEG, CISBIO; now Revvity). Insulin secretion was standardised on the total insulin content of the slices in each chamber. The stimulation index was defined as the ratio of insulin secretion to the mean basal insulin secretion at 3 mmol/l glucose.

Untargeted proteome analysis by LC-MS/MS Fresh frozen tissue samples from the splenic tip site of the pancreas from non-fasted 3- to 4-day-old PHGs and PNGs, in each group derived from different litters and included both sexes, were pulverised using a cryoPREP Automated Dry Pulveriser from Covaris. Proteins were extracted using 8 mol/l urea / 50 mmol/l ammonium bicarbonate buffer supplemented with cOmplete protease inhibitor cocktail (Roche) and

ultrasonication. Protein concentration was determined using the Thermo Pierce 660 nm assay and 50 µg lysate was reduced, alkylated and then digested with Lys-C/trypsin.

LC-MS/MS proteomics was performed on a timsTOF HT mass spectrometer coupled to a nanoElute 2 LC system (both Bruker Daltonics, Bremen, Germany). Peptides were trapped on a PepMap 100 C18 trap column (5 mm × 0.3 mm, 5 µm particles; Thermo Fisher Scientific) and separated on a PepSep ULTRA (25 cm × 75 µm × 1.5 µm; Bruker Daltonics) at 250 nl/min with the following gradient: 2% B to 25% B in 25 min; then to 37% B in 12 min. Solvent A consisted of 0.1% formic acid in water and solvent B of 0.1% formic acid in acetonitrile. The mass spectrometer was run in the dia-PASEF mode using 21 25 m/z wide windows combined with ion mobility ramps between 0.85 and 1.27 1/k0.

A data-independent acquisition (DIA) approach [15] was used to enable accurate and in-depth quantitative proteomic profiling. The data were searched using DIA-NN (v.1.9.2) [22] and the porcine UniProt Reference Proteome UP000008227 (all entries, retrieval date 01.10.2024) as a sequence database. Additionally, common contaminants were added to the sequence database. Only proteins having at least two identified peptides were considered for further quantitative analysis, which was performed using R (v. 4.4.1) [23] and Perseus (v.1.6.7.0) [24]. For this, data were $\log_2$-transformed, then further filtered for at least five valid values in at least one of the groups. Missing values were subsequently imputed from a normal distribution (width=0.3, downshift=1.8). Differentially abundant proteins between PHGs and PNGs were identified using a modified *t* test with correction for multiple testing to a false discovery rate of 5% [25]. To identify relevant candidates and biological processes among the differentially abundant proteins, an overrepresentation analysis was performed using EnrichR.

The dataset has been submitted to the ProteomeXchange Consortium via the PRIDE [26] partner repository with the dataset identifier PXD071507.

Single-cell RNA sequencing analysis of beta cell-enriched pancreas samples The pancreases from non-fasted 1-day-old piglets carrying the *INS*-eGFP transgene were minced into small fragments and then subjected to collagenase digestion as previously described [27]. Animals from different litters were used, and a maximum of two animals were processed per day due to the experimental workflow's capacity. Consequently, complete randomisation was not feasible, and allocation to experimental groups was constrained by the availability of animals with the required genotype, sex and predefined narrow age range. To prepare the isolates for flow cytometry, they underwent an additional digestion with TrypLE (12605, Life Technologies), yielding a single-cell suspension. This suspension was ultimately resuspended in 1–2 ml of flow cytometry buffer (2% FCS, 2 mmol/l EDTA in PBS) and subsequently filtered through the 40 µm cell strainer caps of FACS tubes. A FACS-Aria III instrument (using FACSDiva software v.6.1.3, BD Biosciences) fitted with a 100 µm nozzle was used for sorting GFP-positive cells. For every experiment, single cells were gated based on their FSC area (FSC-A) and SSC area (SSC-A). The gating of singlets was dependent on the FSC width (FSC-W) and FSC height (FSC-H). Non-viable cells were excluded by using 7-AAD (00-6993-50, eBioscience).

Libraries were prepared using the Chromium Single Cell 3′ Reagent Kits v3.1 (1000268, 10x Genomics, Pleasanton, CA, USA) according to the manufacturer's instructions with a targeted cell recovery of 10,000 cells. Libraries were pooled and sequenced on an Illumina NovaSeq6000, aiming for a target read depth of 50,000 reads/cell. FASTQ files were aligned to the Sscrofa11.1 pig genome with improved annotations based on Ensembl release 94 as previously described [10]. The data were then pre-processed using the Cell Ranger software v3.1.0 (10x Genomics) for downstream analyses.

The pre-processing steps for the obtained single-cell RNA-seq (scRNA-seq) data were done using Python 3.9 and the Scanpy package [28] as detailed in the following sections. Each sample was processed independently, with filtering thresholds selected on a per-sample basis. The specific versions of the software packages used are documented in the available Jupyter notebooks (see Data and code availability section).

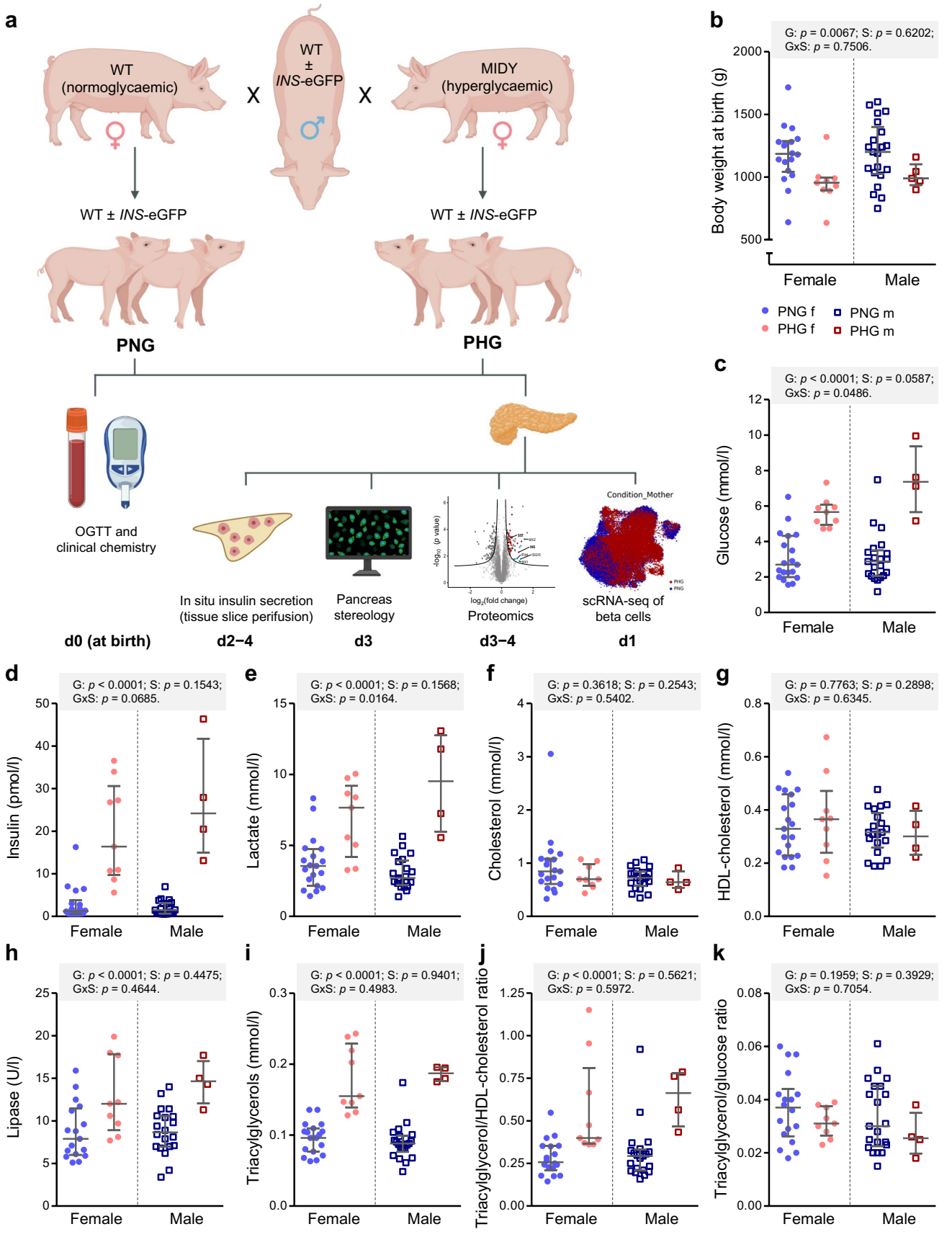
Initial pre-filtering of the raw data from the Cell Ranger pipeline was done with the Scanpy pp.filter_cells and pp.filter_genes functions. This step eliminated cells with fewer than one count and genes detected in fewer than one cell.

For the identification of ambient genes, the R package DropletUtils [29] was used in R 4.3. A *p* value cutoff for ambient genes was set at 0.00065 based on visual inspection.

The R package DropletUtils was also used to identify empty droplets. The output from DropletUtils was then merged with the barcodes from the filtered matrix generated by the Cell Ranger pipeline. The intersection of barcodes from these two sources was then used for subsequent analysis.

Further cell filtering and quality control were performed according to published best practice tutorials [30]. Briefly, cells with excessively low or high count numbers were removed, along with cells containing very few genes. Additionally, cells exhibiting a high percentage of mitochondrial genes were excluded. The exact thresholds used are available in ESM Fig. 2 and the provided notebooks (see Data and code availability).

A total of five different programs were utilised for doublet detection. In this process, each cell was assigned a score of 0–5, reflecting the number of programs that identified it as a doublet. The programs employed were Scrublet [31] and DoubletDetection [32] in Python, and scDblFinder [33], scds [34] and DoubletFinder [35] in R. At this stage, putative doublets were scored but not yet removed from the analysis.


a
WT
(normoglycaemic)
X
WT
±
INS-eGFP
X
MIDY
(hyperglycaemic)
WT ± INS-eGFP
WT ± INS-eGFP
PNG
PHG
OGTT and
clinical chemistry
In situ insulin secretion
(tissue slice perifusion)
Pancreas
stereology
Proteomics
Condition_Mother
scRNA-seq of
beta cells
d0 (at birth)
d2–4
d3
d3–4
d1
b
G: p = 0.0067; S: p = 0.6202;
GxS: p = 0.7506.
Body weight at birth (g)
Female
Male
PNG f
PNG m
PHG f
PHG m
c
G: p < 0.0001; S: p = 0.0587;
GxS: p = 0.0486.
Glucose (mmol/l)
d
G: p < 0.0001; S: p = 0.1543;
GxS: p = 0.0685.
Insulin (pmol/l)
e
G: p < 0.0001; S: p = 0.1568;
GxS: p = 0.0164.
Lactate (mmol/l)
f
G: p = 0.3618; S: p = 0.2543;
GxS: p = 0.5402.
Cholesterol (mmol/l)
g
G: p = 0.7763; S: p = 0.2898;
GxS: p = 0.6345.
HDL-cholesterol (mmol/l)
h
G: p < 0.0001; S: p = 0.4475;
GxS: p = 0.4644.
Lipase (U/l)
i
G: p < 0.0001; S: p = 0.9401;
GxS: p = 0.4983.
Triacylglycerols (mmol/l)
j
G: p < 0.0001; S: p = 0.5621;
GxS: p = 0.5972.
Triacylglycerol/HDL-cholesterol ratio
k
G: p = 0.1959; S: p = 0.3929;
GxS: p = 0.7054.
Triacylglycerol/glucose ratio

◂**Fig. 1** Experimental design, birthweights and clinical-chemical variables of PHGs vs PNGs. (**a**) Study design to assess the impact of maternal diabetes on metabolism and beta cell health, with the age of the piglets on the days on which the various analyses were performed (d0–d4) indicated. Created in BioRender. Kemter, E. (2026) https://BioRender.com/br06ynf. (**b**) Birthweights of PHGs and PNGs. (**c**–**k**) Clinical-chemical parameters from PHGs (9 females, 4 or 5 males) and PNGs (18 or 19 females, 21 males) based on plasma collected 30 min after birth. Data are presented as scatter dot plot with median lines and IQR. *p* values were calculated using PROC GLM. f, female; G, group (diabetic vs non-diabetic mother); m, male; S, sex of the piglet

The individual samples were combined, and only genes detected across all samples were retained. To correct for variations in sequencing depth, the combined object was normalised using the scran package in R [36]. Following normalisation, the values were log-transformed (log[expr+1]).

Sample integration was performed using scvi-tools [37]. Initially, the top 4000 highly variable genes (HVGs) were identified via Scanpy, with the flavor="seurat" setting and individual samples designated as batches. Any potential ambient genes (see above) were removed from the HVG list. Subsequently, a scvi model was trained on these filtered HVGs using the following settings: batch_key='sample'; layer='raw_counts'; 20 latent dimensions; 256 hidden layers; a gene-batch dispersion model; a zinb gene_likelihood; and a normal latent_distribution.

To generate a Uniform Manifold Approximation and Projection (UMAP) [38], a neighbourhood graph of the cells was constructed using the pp.neighbors function in Scanpy, configured with n_neighbors =25, n_pcs =20, and metric=correlation. The UMAP was then computed in Scanpy with default parameters, except for min_dist =0.2.

To eliminate potential doublets from subsequent analysis, high-resolution Leiden clustering [39], as implemented in Scanpy, was run with a resolution =2. Any resulting clusters where over 70% of cells were marked as doublets by at least one method, and over 30% were marked as doublets by at least two methods, were excluded. Following this, any remaining cells identified as doublets by three or more methods were also removed. The UMAP was then recalculated using standard Scanpy parameters.

The R package clustree [39] was used to visualise and compare various Leiden clustering resolutions. For annotation purposes, a resolution of 1.3 was selected. Cycling cells were identified by scoring genes associated with the S and G2M phases of the cell cycle using the Scanpy implementation [40]. Cell types were assigned based on established marker genes (ESM Fig. 2f), which were scored using the tl.score_genes function in Scanpy. The clusters were subsequently named according to these marker gene scores.

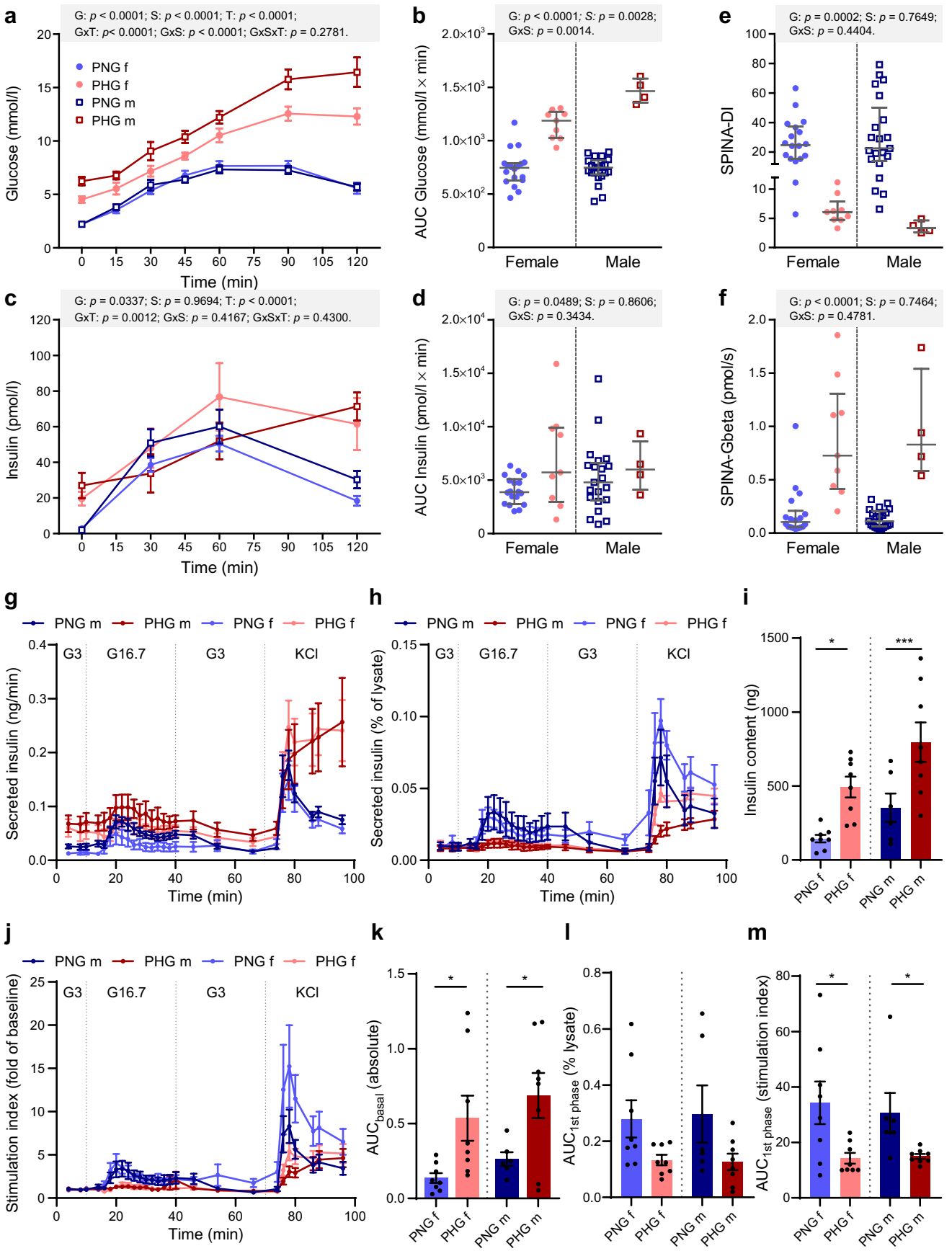
A differential gene expression analysis was conducted to compare PNG samples with PHG samples. This comparison was performed using DElegate [41], which generates pseudobulks and serves as a wrapper for edgeR [42].

The beta cells were sub-clustered in 'rp_high' and 'rp_low' fractions according to the fraction of expressed ribosomal genes using two independent unsupervised separations: (1) a per-cell threshold (rp_frac <0.03); and (2) a Leiden re-clustering with assignment by cluster-mean rp_frac.

Venn diagrams were created using matplotlib-venn based on the results of the differential gene expression analyses.

Immunostaining of pancreas tissue After dewaxing of 3 µm thick slides from 4% PFA-fixed paraffin-embedded pancreatic tissues, heat-induced epitope retrieval was performed either in 10 mmol/l citrate buffer (pH 6.0) or in 10 mmol/l Tris/1 mmol/l EDTA buffer (pH 9.0), both supplemented with 0.05% Tween20 (Sigma-Aldrich), for 15 min or 18 min, respectively, in a microwave. After a 30 min cooling period, slides were transferred to 1× PBS for 10 min, followed by incubation in 1× PBS-Triton X100 0.1% for 10 min, and then again in 1× PBS for 5 min, before slides were blocked in a 1× PBS-Tween20 0.05% solution containing 5% donkey serum for 1 h at room temperature in a humidified chamber. Details of the antibody incubation steps, the slide-washing series and immunofluorescence slide processing before microscopy are listed in ESM Table 1, along with all primary and secondary antibodies used in this study. For selected primary antibodies, specificity was verified by western blotting to confirm detection of the porcine target protein in previous studies (e.g. phospho-mTOR). For all antibodies, staining patterns were assessed for consistency with the reported cell-type specificity and intracellular distribution in the Human Protein Atlas and/or the literature. Only antibodies that specifically detected the porcine target protein and showed consistent immunohistochemical staining patterns across all animals tested (n=3 per group, including both sexes) were included in the analysis to ensure reproducibility across animals. Images were acquired using a Leica SP8 confocal microscope with 20× glycerol or 40× water immersion objectives or, for whole-slide images (WSIs), a ZEISS Axioscan 7 slide scanner microscope with 20× objective.

Quantitative image analysis Digital image analysis was performed on WSIs using QuPath open-source software (v0.4.4) [43], as described elsewhere [44]. Image analysis was performed in a blinded manner to the experimental group, with group identities masked throughout the analysis. Slides were co-stained for glucagon (GCG), insulin, somatostatin (SST) and pancreatic polypeptide (PPY) and counterstained with DAPI for visualisation of nuclei. Axioscan 7 image acquisition was performed using the appropriate laser lanes for DAPI, AF488, AF555, AF633 and AF750, with a resolution of 0.344 µm per pixel. Images were imported into


a
G: p < 0.0001; S: p < 0.0001; T: p < 0.0001;
GxT: p< 0.0001; GxS: p < 0.0001; GxSxT: p = 0.2781.
PNG f
PHG f
PNG m
PHG m
Glucose (mmol/l)
Time (min)
b
G: p < 0.0001; S: p = 0.0028;
GxS: p = 0.0014.
AUC Glucose (mmol/l × min)
Female
Male
e
G: p = 0.0002; S: p = 0.7649;
GxS: p = 0.4404.
SPINA-DI
Female
Male
c
G: p = 0.0337; S: p = 0.9694; T: p < 0.0001;
GxT: p = 0.0012; GxS: p = 0.4167; GxSxT: p = 0.4300.
Insulin (pmol/l)
Time (min)
d
G: p = 0.0489; S: p = 0.8606;
GxS: p = 0.3434.
AUC Insulin (pmol/l × min)
Female
Male
f
G: p < 0.0001; S: p = 0.7464;
GxS: p = 0.4781.
SPINA-Gbeta (pmol/s)
Female
Male
g
PNG m
PHG m
PNG f
PHG f
G3
G16.7
G3
KCl
Secreted insulin (ng/min)
Time (min)
h
PNG m
PHG m
PNG f
PHG f
G3
G16.7
G3
KCl
Secreted insulin (% of lysate)
Time (min)
i
Insulin content (ng)
*
***
PNG f
PHG f
PNG m
PHG m
j
PNG m
PHG m
PNG f
PHG f
G3
G16.7
G3
KCl
Stimulation index (fold of baseline)
Time (min)
k
AUCbasal (absolute)
*
*
PNG f
PHG f
PNG m
PHG m
l
AUC1st phase (% lysate)
PNG f
PHG f
PNG m
PHG m
m
AUC1st phase (stimulation index)
*
*
PNG f
PHG f
PNG m
PHG m

◂**Fig. 2** Assessment of glucose sensitivity and insulin secretion in vivo and on viable pancreatic tissue slices in situ. (**a**–**d**) OGTT in neonatal PHGs and PNGs prior to first colostrum intake; blood glucose (**a**) and plasma insulin levels (**c**), and their respective AUCs (**b**, **d**), are shown. PHGs, 9 females, 4 or 5 males; PNGs, 18 females, 21 males. (**e**, **f**) Surrogate marker for insulin–glucose homeostasis (**e**, SPINA-DI) and beta cell function (**f**, SPINA-Gbeta). (**g**–**m**) Dynamic GSIS of viable pancreas tissue slices from 2- to 4-day-old PHGs (4 males, 4 females) and PNGs (3 males, 4 females): absolute amount of secreted insulin per slice (**g**); secreted insulin standardised to insulin content (**h**); secreted insulin standardised to basal insulin at 3 mmol/l glucose (**j**); absolute insulin content of tissue slices (**i**); AUC of secreted insulin from basal (3 mmol/l glucose) insulin curve (**k**); AUC of secreted insulin from first-phase response curve, expressed as percentage of lysate (**l**) or normalised to basal insulin secretion at 3 mmol/l glucose (**m**). The TP of change from 3 mmol/l glucose, 16.7 mmol/l glucose, and 16.7 mmol/l glucose plus KCl, respectively, and duration of perifusion are indicated. Time on *x*-axes is shown relative to glucose administration. Data are shown as mean ± SEM (**a**, **c**, **g**, **h**, **j**), as scatter dot plot with median lines and IQR (**b**, **d**–**f**), and as scatter dot plot with mean lines and SEM (**i**, **k**–**m**). *$p<0.05$, ***$p<0.001$ [calculated by ANOVA (**a**–**d**) and unpaired *t* test (**i**, **k**–**m**)]. f, female; G, group (diabetic vs non-diabetic mother); G3, 3 mmol/l glucose; G16.7, 16.7 mmol/l glucose; m, male; S, sex (of the piglet)

QuPath as fluorescence image types. Tissue was detected using a threshold pixel classifier, which was then manually adjusted to exclude regions of artefacts such as folding or air bubbles. For islet detection, a pixel classifier was trained using QuPath's machine learning tool on the four channels: GCG; INS; SST; and PPY. An object classifier was trained for cell-type identification and combined into composite classifiers. Annotations of islets, cell counts and cell types were exported to Excel. Islet size distribution (total number of islets containing at least one endocrine cell count) and number of islets separated for number of endocrine cell counts (1–5, 6–10, 11–20, 21–40, >40) were calculated. The percentage of islets of each size category was calculated from the total number of islets (=100%). The endocrine cell content was calculated as the percentage of each endocrine cell type in the total number of pancreas cells (=100%).

Statistical analysis A power calculation was performed for the three biologically most relevant endpoints: (1) neonatal fasting glucose; (2) neonatal fasting insulin; and (3) glucose AUC during the OGTT. For each endpoint, a large standardised effect size of Cohen's $d=1.7$ was assumed. Because maternal diabetes status is a sow-level exposure, litter represents the primary independent experimental unit. Nevertheless, measurements from multiple piglets within a litter provided additional information because individual piglets differ genetically and may experience different intrauterine conditions. These observations are not fully independent, however, because offspring from the same litter share their maternal environment and part of their genetic background. Litter clustering was therefore incorporated into the power calculation using an assumed intraclass correlation coefficient (ICC) of 0.40. The effective sample size (n_{eff}) was calculated as $n_{\text{eff}} = \frac{n}{1+(\overline{m}-1)\text{xICC}}$, with n=no. of piglets and $\overline{m}$ =mean litter size. The diabetic group comprised five litters and 13 offspring, corresponding to a mean of 2.6 offspring per litter. Using the design-effect approximation, this resulted in an effective sample size of 7.9. The non-diabetic control group comprised four litters and 39 offspring, corresponding to a mean of 9.75 offspring per litter and an effective sample size of 8.7. Assuming a two-sided significance level of $\alpha=0.05$, Cohen's $d=1.7$, and inference based on the nine independent litters, the estimated power for each endpoint was approximately 84%, demonstrating that our studies were sufficiently powered.

Glucose and insulin levels during OGTT were evaluated by ANOVA (Linear Mixed Models; SAS 8.2) taking the fixed effects of group (diabetic vs non-diabetic mother), sow (nested within group), sex (of the piglet), time (relative to glucose administration), the interactions group × sex, group × time, and group × sex × time, as well as the random effect of the individual piglet into account. PROC GLM (General Linear Models, SAS 8.2) was used to analyse body and organ weight data, all quantitative stereology parameters of the pancreas, and clinical-chemical variables, except OGTT. Least squares means (LSMs) and SEs of LSMs were calculated for group × sex × time and compared using Student's *t* test. AUC and insulin content of dynamic GSIS of tissue slices were evaluated by Student's *t* test using GraphPad Prism 10 software. GraphPad Prism software (versions 5.02 and 10.1.2) was used to generate figures and calculate AUC values, means and SEMs. Significance was defined as $p<0.05$.

Statistical analyses of LC-MS/MS and scRNA-seq data are covered in the corresponding methods subsections.

No data were excluded except those with technical failure. During scRNA-seq data processing, low quality cells were excluded to maintain high quality datasets for downstream analysis to derive meaningful results.

Results

A translational model for studying the effects of maternal diabetes on islet pathophysiology in neonatal offspring On the maternal side, we used a non-obese, genetically diabetic (*INS*^{C94Y} transgenic) pig model [11], a translational large-animal model for MIDY that clinically resembles the human 'severe insulin-deficient diabetes' (SIDD) subtype of type 2 diabetes [45] most closely. The pregestational diabetes in this model, therefore, also encompasses the developmental impact of intrauterine hyperglycaemia during the first trimester, when pancreas organogenesis and beta cell

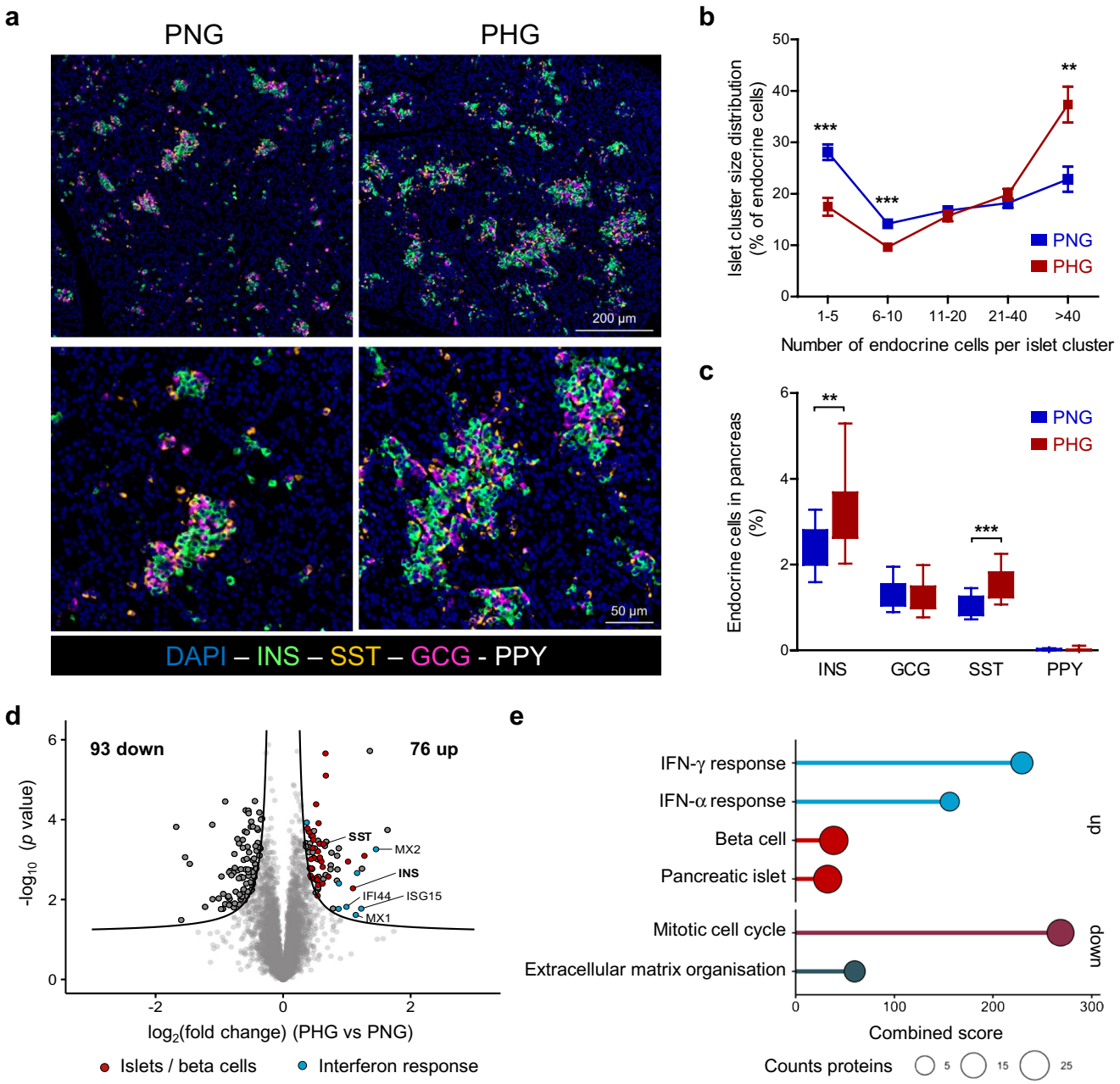


Fig. 3 Morphological assessment of islet size and composition, and untargeted proteome analysis of pancreas from PHGs vs PNGs. (**a**) Representative images of pancreas tail region, stained for insulin, GCG, SST and PPY, from 3-day-old PHGs and PNGs. Scale bar, 200 µm (top) or 50 µm (bottom). (**b**, **c**) Islet size distribution (**b**) and relative endocrine cell content (**c**) in pancreas tail region in PNGs (n=13) and PHGs (n=14). Data are presented as mean ± SEM, with the number of endocrine cells per cluster as indicated (**b**), and as box plots with 5–95th percentile ranges (whiskers) (**c**). **p<0.01, ***p<0.001 (calculated using PROC GLM). (**d**) Volcano plot comparing pancreas protein abundance between PNGs and PHGs. The x- and y-axis show the $\log_2$ fold change in protein levels and the $-\log_{10}$ p value, respectively. Proteins above the drawn curve are considered significant. The curve was calculated based on a modified t test and enforces a false discovery rate of <0.05. Selected proteins are annotated with gene names and colour-coded according to the corresponding biological processes. (**e**) Selected terms from the enrichment analysis that are over-represented in the differentially abundant proteins from the untargeted pancreas proteome analysis. INS, insulin

development occur [10] (ESM Fig. 1). Hemizygous *INS*^{C94Y} transgenic or WT sows were crossed with either a WT boar or with a boar carrying an *INS*-eGFP transgene [12] as a fluorescent marker for beta cell isolation. Analyses were performed on WT/*INS*-eGFP piglets born to normoglycaemic mothers (PNGs) and WT/*INS*-eGFP piglets born

to hyperglycaemic mothers (PHGs). This study focused on glucose and insulin metabolism in newborn offspring during the first 3 days of life, being the transition period from constant placental nutrient supply to intermittent postnatal feeding. The study design is shown in Fig. 1a.

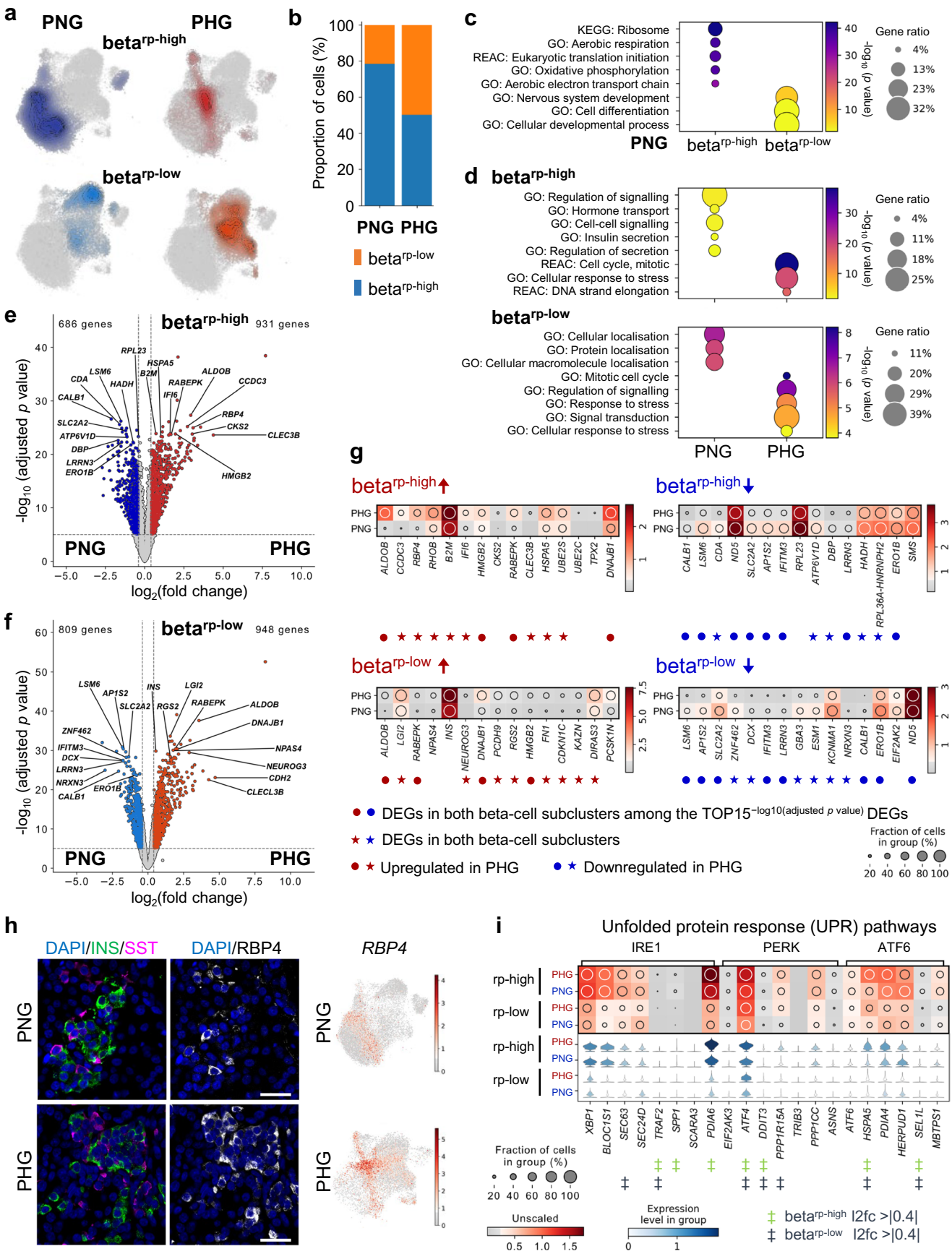
Metabolic alterations were more severe in male than in female offspring of diabetic mothers The metabolic health of newborn offspring was evaluated in offspring from five litters of diabetic and four litters of non-diabetic sows on the day of birth. Litter size of non-diabetic mothers ranged from 8 to 14 piglets (mean 11.6), whereas diabetic sows gave birth to 7–12 piglets (mean 8.4). Body weights at birth were distinctly lower in PHGs than in PNGs (Fig. 1b). While absolute organ weights were smaller in PHGs than in PNGs, relative organ weights (except for the heart, brain and kidneys) were similar between the groups (ESM Fig. 3).

Shortly after birth, before the first milk intake, blood levels of glucose, insulin, lactate, triacylglycerols, and the triacylglycerol:HDL-cholesterol ratio were elevated twofold or more in PHGs (Fig. 1c–k), indicating that exposure to maternal hyperglycaemia in uterine life negatively affects neonatal energy and lipid metabolism. During the OGTT, PNGs reached peak blood glucose levels at 60–90 min after oral glucose intake (Fig. 2a). PHGs showed peak blood glucose levels at 90–120 min, indicating impaired glucose tolerance. Notably, blood glucose levels before glucose/colostrum intake were distinctly higher in male than in female PHGs (mean ± SD: 134.4 ± 35.4 vs 120.0 ± 59.6 mg/dl; $p<0.05$ for the group × sex interaction), and glucose levels of male PHGs remained consistently higher after oral glucose intake. In contrast, no significant sex-related differences were observed in the PNG group. The AUC for glucose levels was significantly higher in PHGs than in PNGs and higher in male PHGs than in female PHGs (Fig. 2b). Fasting insulin levels were significantly elevated in both male and female PHGs, and the insulin response during the OGTT was also significantly altered in PHGs compared with PNGs (Fig. 2c). A sex-specific difference in the insulin response curve was observed in PHGs, with males showing a delayed rise in insulin levels that continued until the end of the OGTT (120 min). In contrast, female PHGs reached peak insulin levels 60 min after glucose ingestion. At 120 min, insulin levels in both male and female PHGs were higher than in PNGs. Overall, the AUC for insulin levels was higher in PHGs than in PNGs (Fig. 2d). Indexes calculated from blood glucose and insulin levels during the OGTT, such as SPINA-GR and SPINA-Gbeta, indicated reduced insulin sensitivity and impaired beta cell secretory function in PHGs (Fig. 2e, f and ESM Fig. 4).

Fetal pancreas development in a hyperglycaemic environment leads to impaired regulated insulin secretion in neonates To evaluate beta cell function, we measured insulin secretion kinetics in situ from viable pancreatic tissue slices obtained from neonatal piglets under near-physiological conditions (Fig. 2g–m). Interestingly, AUC values during basal secretion were significantly higher in PHG than in PNG samples (2.6-fold in males, 3.9-fold in females) (Fig. 2g, k). Because absolute hormone secretion from tissue slices cannot be standardised, insulin secretion was normalised to the total insulin content of the samples (Fig. 2h, i) or to basal secretion (Fig. 2j, k). The overall insulin content was significantly higher in PHG compared with PNG samples, irrespective of sex (Fig. 2i), which explains the higher basal insulin secretion observed in PHG samples. However, stimulation with 16.7 mmol/l glucose did not induce a major increase in insulin secretion (Fig. 2h, j). The near-complete blunting of first-phase insulin secretion was evident with both normalisation methods (Fig. 2l, m). In addition, the normalised maximal secretory output in response to KCl stimulation was reduced in PHG samples. These results suggest that islets chronically exposed to hyperglycaemia during fetal development are unable to respond adequately to a glucose load and already exhibit signs of early dysfunction. Consequently, oral glucose intake failed to elicit a timely insulin response, resulting in a distinct delay in both glucose and insulin responses in PHGs.

Increased islet size and increased proportions of beta and delta cells in pancreas of PHGs Next, we performed histomorphological analyses of the pancreatic tail regions from neonatal PHGs and PNGs (Fig. 3a–c). The pancreas of neonatal piglets is still immature, with more than 40% of endocrine cells distributed as solitary cells or small clusters of fewer than ten cells within the exocrine compartment. Compared with PNG samples, endocrine cells in PHG samples were organised into larger clusters, and a higher proportion of endocrine cells was located within the islets of Langerhans. In addition, pancreases of PHGs contained higher proportions of insulin-positive beta cells and SST^+ delta cells than pancreases from PNGs, whereas the proportions of GCG^+ alpha cells and PPY^+ cells were similar between groups (Fig. 3c). These findings suggest that exposure to a hyperglycaemic and hyperinsulinaemic intrauterine environment increases the proportions of beta cells and delta cells to compensate for increased metabolic demands.

Elevated abundance of islet proteins and inflammasome-associated changes in the neonatal pancreatic proteome of PHGs To gain deeper insight into the molecular changes induced by maternal diabetes, we next performed


a
PNG
PHG
beta^rp-high
beta^rp-low
b
Proportion of cells (%)
PNG PHG
beta^rp-low
beta^rp-high
c
KEGG: Ribosome
GO: Aerobic respiration
REAC: Eukaryotic translation initiation
GO: Oxidative phosphorylation
GO: Aerobic electron transport chain
GO: Nervous system development
GO: Cell differentiation
GO: Cellular developmental process
PNG
beta^rp-high
beta^rp-low
-log10 (p value)
Gene ratio
4%
13%
23%
32%
d
beta^rp-high
GO: Regulation of signalling
GO: Hormone transport
GO: Cell-cell signalling
GO: Insulin secretion
GO: Regulation of secretion
REAC: Cell cycle, mitotic
GO: Cellular response to stress
REAC: DNA strand elongation
4%
11%
18%
25%
beta^rp-low
GO: Cellular localisation
GO: Protein localisation
GO: Cellular macromolecule localisation
GO: Mitotic cell cycle
GO: Regulation of signalling
GO: Response to stress
GO: Signal transduction
GO: Cellular response to stress
11%
20%
29%
39%
PNG
PHG
e
686 genes
beta^rp-high
931 genes
-log10 (adjusted p value)
log2(fold change)
PNG
PHG
RPL23
HSPA5
B2M
ALDOB
CDA
LSM6
HADH
RABEPK
CCDC3
CALB1
IFI6
RBP4
SLC2A2
CKS2
ATP6V1D
CLEC3B
DBP
LRRN3
ERO1B
HMGB2
f
809 genes
beta^rp-low
948 genes
-log10 (adjusted p value)
log2(fold change)
PNG
PHG
LSM6
AP1S2
INS
LGI2
SLC2A2
RGS2
RABEPK
ALDOB
DNAJB1
ZNF462
NPAS4
IFITM3
DCX
NEUROG3
LRRN3
CDH2
NRXN3
CLECL3B
CALB1
ERO1B
g
beta^rp-high ↑
beta^rp-high ↓
beta^rp-low ↑
beta^rp-low ↓
PHG
PNG
ALDOB CCDC3 RBP4 RHOB B2M IFI6 HMGB2 CKS2 RABEPK CLEC3B HSPA5 UBE2S UBE2C TPX2 DNAJB1
CALB1 LSM6 CDA ND5 SLC2A2 AP1S2 IFITM3 RPL23 ATP6V1D DBP LRRN3 HADH ERO1B SMS RPL36A-HNRNPH2
ALDOB LGI2 RABEPK NPAS4 INS NEUROG3 DNAJB1 PCDH9 RGS2 HMGB2 FN1 CDKN1C KAZN DIRAS3 PCSK1N
LSM6 AP1S2 SLC2A2 ZNF462 DCX IFITM3 LRRN3 GBA3 ESM1 KCNMA1 NRXN3 CALB1 ERO1B EIF2AK2 ND5
●● DEGs in both beta-cell subclusters among the TOP15−log10(adjusted p value) DEGs
★★ DEGs in both beta-cell subclusters
●★ Upregulated in PHG
●★ Downregulated in PHG
Fraction of cells in group (%)
20 40 60 80 100
h
DAPI/INS/SST
DAPI/RBP4
RBP4
PNG
PHG
i
Unfolded protein response (UPR) pathways
IRE1
PERK
ATF6
rp-high
rp-low
PHG
PNG
XBP1 BLOC1S1 SEC63 SEC24D TRAF2 SPP1 SCARA3 PDIA6 EIF2AK3 ATF4 DDIT3 PPP1R15A TRIB3 PPP1CC ASNS ATF6 HSPA5 PDIA4 HERPUD1 SEL1L MBTPS1
Fraction of cells in group (%)
20 40 60 80 100
Unscaled
0.5 1.0 1.5
Expression level in group
0 1
‡ beta^rp-high |2fc >|0.4|
‡ beta^rp-low |2fc >|0.4|

◂**Fig. 4** scRNA-seq analysis reveals a distinct beta cell subcluster in PHGs and a molecular profile of dysfunction and stress adaptation. (**a**) UMAP representation of beta cell subclusters for PHGs (red) and PNGs (blue) in the scRNA-seq data. (**b**) Stacked bar chart showing the proportions of beta$^{rp\text{-}high}$ and beta$^{rp\text{-}low}$ cell subclusters in PHGs and PNGs, demonstrating a shift in cell fraction. (**c**, **d**) Top eight enriched terms from enrichment analyses of DEGs in beta$^{rp\text{-}high}$ and beta$^{rp\text{-}low}$ cells of PNGs (**c**), and between PHGs and PNGs in beta$^{rp\text{-}high}$ cells and beta$^{rp\text{-}low}$ cells (**d**), respectively. (**e**, **f**) Volcano plots comparing changes in transcript abundance between PNGs and PHGs in beta$^{rp\text{-}high}$ (**e**) and beta$^{rp\text{-}low}$ (**f**) cells. (**g**) Dot plot showing expression of the top 15 DEGs with the highest $-\log_{10}$(adjusted *p* value) in both beta cell subclusters. Genes with ENSSSCG annotation were excluded. Colour intensity indicates mean expression within a cluster, and dot size indicates the proportion of cells in the cluster expressing the gene. (**h**) Representative immunofluorescence confocal images of pancreas stained for insulin/SST/RBP4, with UMAP plots for *RBP4*. RBP4 is a marker for dysfunctional beta cells. Animals' age: 3 days. Scale bar, 20 μm. (**i**) Dot plots and violin plots of marker genes of UPR pathways. Colour intensity indicates mean expression in a cluster, and dot size indicates the proportion of cells in a cluster expressing the gene. INS, insulin; l2fc, $\log_2$(fold change)

label-free LC-MS/MS proteomics of pancreatic tail tissue samples from 3-day-old PHGs and PNGs. From the 5916 proteins identified, 169 proteins were differentially abundant between PHG and PNG samples (false discovery rate <5%), with 76 proteins increased and 93 decreased in PHG samples (Fig. 3d and ESM Table 2). Notably, the abundances of both insulin and SST were increased ($\log_2$[fold change] +1.10 and +0.63, respectively), consistent with the higher proportions of insulin-positive beta cells (+35%) and SST$^+$ delta cells (+47%) in the PHG pancreatic samples (Fig. 3c). Over-representation analysis (Fig. 3e and ESM Table 2d) revealed that 23 proteins with increased abundance in pancreases of PHGs were associated with beta cells, along with an additional eight proteins associated with pancreatic islets. Notably, several proteins involved in insulin synthesis and processing and intracellular zinc ion homeostasis were also over-represented in PHG samples. Another group of proteins over-represented in PHG samples is involved in IFN-γ signalling (ZBP1; OAS2; MX2; DHX58; MX1; TRIM25; IFI44; ISG15; SRI) or IFN-α signalling (DHX58; MX1; TRIM25; IFI44; ISG15). Notably, MX2, ISG15 and IFI44 were also increased in abundance in liver samples from PHGs [15], suggesting a systemic upregulation of inflammatory signalling in PHGs, reminiscent of the chronic low-grade 'meta-inflammatory' state associated with maternal diabetes [46]. Taken together, these results suggest that islet architecture and cell-type composition, and the inflammatory status, are distinctly altered at birth following exposure to a diabetogenic intrauterine environment. However, because endocrine cells account for only a small fraction of the total pancreatic lysate analysed by LC-MS/MS, no further conclusions can be drawn.

A unique beta cell subcluster positively adapted to chronic hyperglycaemic stress in PHGs To explore the molecular alterations underlying hyperinsulinaemia and the impaired ability of beta cells of PHGs to respond appropriately to a glucose stimulus, we performed scRNA-seq. Beta cells were enriched from pancreatic samples from 1-day-old PHGs and PNGs by FACS based on the expression of the *INS*-eGFP reporter transgene. After quality control, a total of 39,392 cells were retained, of which 17,631 and 13,511 were annotated as beta cells from PNG and PHG samples, respectively (ESM Fig. 2). Notably, the abundance of nearly all detected transcripts of ribosomal genes was lower in beta cells from PHGs than in beta cells from PNGs (Fig. 4a, ESM Figs 5, 6 and ESM Table 3). We therefore identified two distinct beta cell populations that differed in their ribosomal gene transcript content: beta cells with high ribosomal gene transcript content (beta$^{rp\text{-}high}$); and beta cells with low ribosomal gene transcript content (beta$^{rp\text{-}low}$). Whereas nearly 80% of the beta cells from PNGs exhibited high ribosomal gene transcript expression, PHG samples showed a pronounced shift toward the beta$^{rp\text{-}low}$ subpopulation, with approximately half of the beta cells belonging to this cluster (Fig. 4b). This effect of maternal diabetes on ribosomal gene transcript abundance was beta cell specific as it was not observed in other pancreatic cell types, except for a moderate shift toward rp-low cells in the NGN3–FEV endocrine progenitor population and in ductal cells (ESM Fig. 5c). Over-representation analysis of genes differentially expressed between beta$^{rp\text{-}high}$ and beta$^{rp\text{-}low}$ cells in PNG samples revealed transcript enrichment for genes involved in protein translation and mitochondrial ATP production (Fig. 4c and ESM Table 4). In contrast, beta$^{rp\text{-}low}$ cells showed enrichment of transcripts associated with cell differentiation.

To assess whether the beta$^{rp\text{-}low}$ subcluster identified in our study resembles previously reported beta cell subclusters, we examined the transcript profiles of known subtype markers in our neonatal pig dataset (ESM Fig. 6). Transcripts of *CD9,* encoding a surface marker that together with ST8SIA1 differentiates human beta cell populations [47], were distinctly more abundant in beta$^{rp\text{-}high}$ cells and were nearly absent in beta$^{rp\text{-}low}$ cells. In contrast, *ST8SIA1* transcripts were detected only in a few pig beta cells. The transcription factor RFX6, identified in a type 2 diabetes genome-wide association study as a network module factor with low RFX6 expression linked to increased type 2 diabetes risk [48], showed higher transcript levels in beta$^{rp\text{-}low}$ cells than in beta$^{rp\text{-}high}$ cells. This transcript distribution pattern was also seen for another transcription factor, MYT1, a marker that distinguished two nutritionally regulated neurogenin-3-derived beta cell subclusters in mice [49]. However, drawing further conclusions is limited because these subcluster comparisons were conducted at the transcript level.

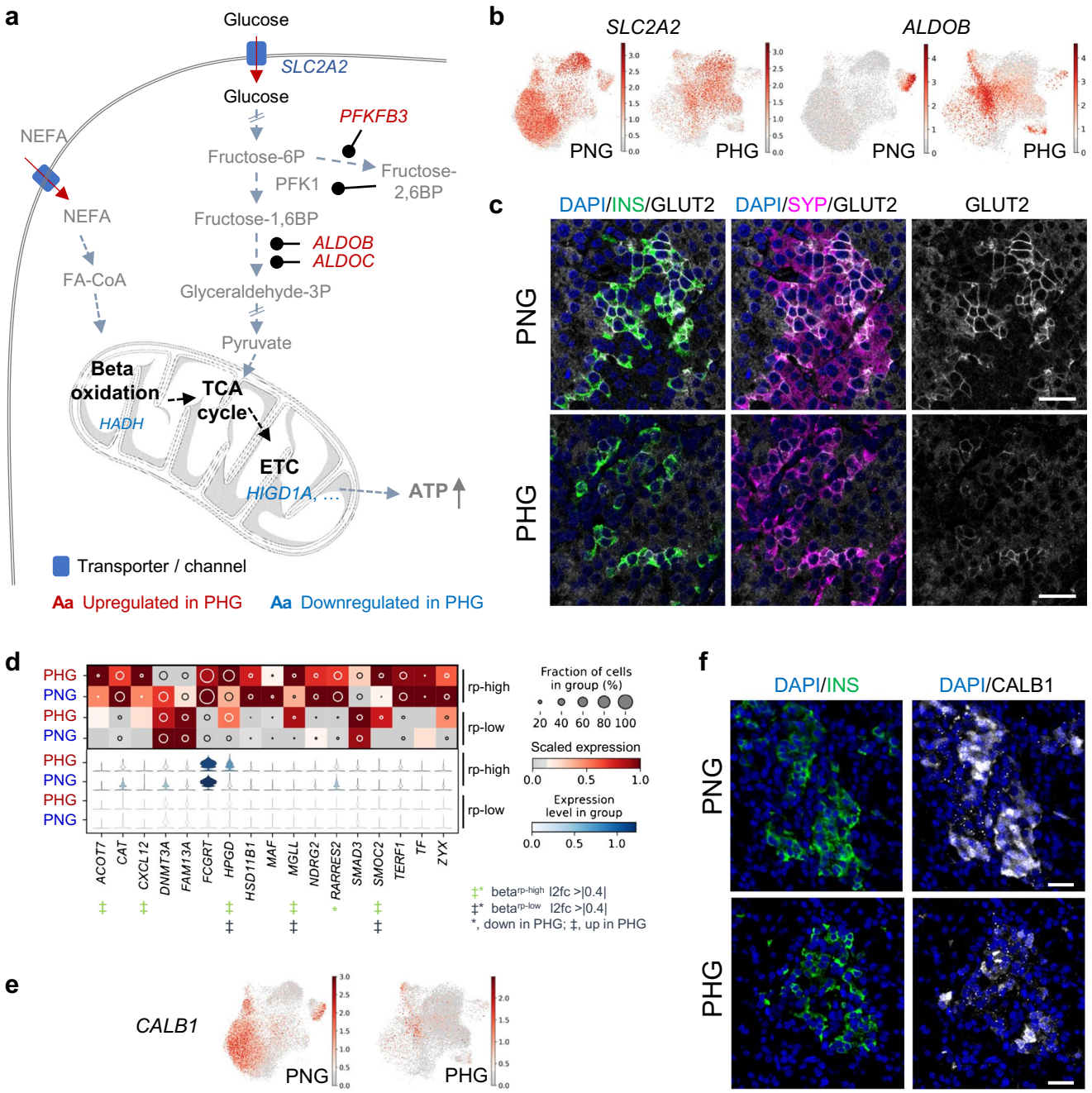


Fig. 5 Hallmarks of nutrient metabolism changes and disturbed calcium buffer system in beta cells from PHGs. (**a**) Schematic overview of nutrient metabolism with focus on glucose uptake and glycolysis in beta cells. Created in BioRender. Kemter, E. (2026) https://BioRender.com/br06ynf. (**b**) UMAP plots for *SLC2A2* and *ALDOB*. (**c**) Demonstration of nearly absent GLUT2 transporter in beta cells from PHGs by representative immunofluorescence images. Animals' age: 3 days. Scale bar, 20 µm. (**d**) Dot plots and violin plots of disallowed genes in beta cells. Colour intensity indicates mean expression in a cluster, and dot size indicates the proportion of cells in a cluster expressing the gene. Expression is scaled per gene. (**e**) UMAP plots for *CALB1*. (**f**) Representative immunofluorescence images demonstrating the near absence of calbindin D28K in most beta cells from PHGs, indicating disturbed calcium homeostasis. Animals' age: 3 days. Scale bar, 20 µm. CALB1, calbindin D28K; ETC, electron transport chain; INS, insulin; l2fc, $\log_2$(fold change); SYP, synaptophysin (a marker to visualise endocrine cells); TCA cycle, citrate cycle

Next, we focused on the differentially expressed genes (DEGs) between PHGs and PNGs. In total, 1617 and 1757 DEGs were gene-annotated in beta$^{rp\text{-}high}$ and beta$^{rp\text{-}low}$ cells, respectively (Fig. 4d–f and ESM Tables 5, 6). Nearly half of the DEGs in beta$^{rp\text{-}high}$ cells were also differentially expressed in the same direction in beta$^{rp\text{-}low}$ cells (ESM

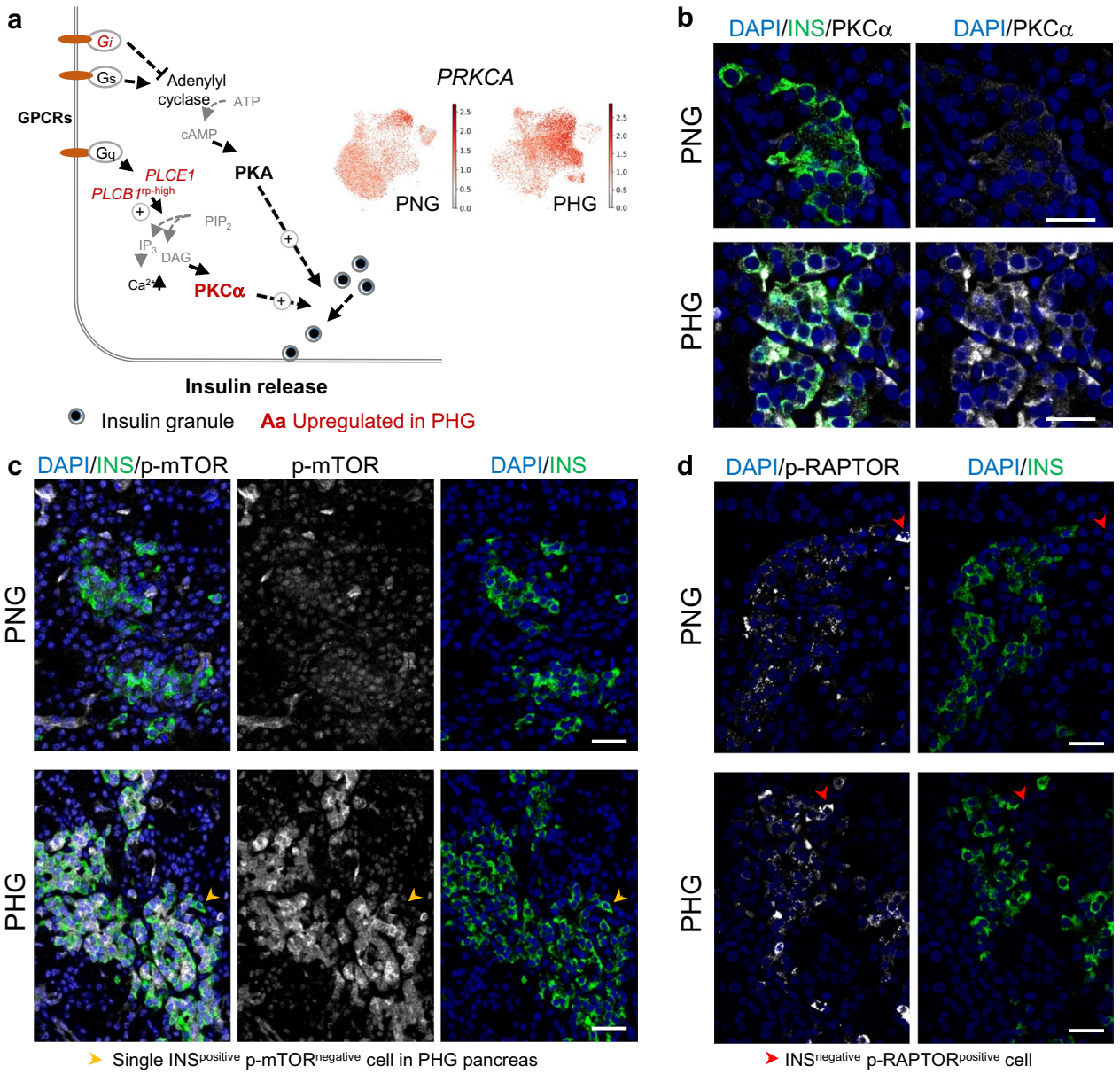
Fig. 7), indicating a profound impact of maternal diabetes on the offspring's beta cell transcriptome. Although several genes associated with beta cell maturity or immaturity showed differential transcript abundance between PHG and PNG, beta cell identity and maturity status in both groups appeared similar (ESM Fig. 8). Over-representation analysis indicated that in PHGs the DEGs were enriched in processes such as the mitotic cell cycle and cellular stress responses. In addition, subcluster-specific effects of maternal diabetes were evident, including the regulation of insulin secretion, which was negatively affected in the beta$^{rp\text{-}high}$ cell transcriptome. The functional category 'regulation of signalling' differed between the subclusters: related transcripts were under-represented in beta$^{rp\text{-}high}$ cells of PHGs but over-represented in beta$^{rp\text{-}low}$ cells of PHGs. Together, these findings indicate global and subcluster-specific transcriptomic changes in PHG beta cells, alongside a shift in subcluster proportions.

To obtain a more detailed overview of key alterations in beta cells of PHGs, we next focused on the top 15 DEGs with the highest adjusted log(p values) in beta$^{rp\text{-}high}$ and beta$^{rp\text{-}low}$ cells of PHGs vs PNGs (Fig. 4g). Although the overlap among the top 15 DEGs was limited between the two beta cell subclusters, most DEGs showed concordant differential expression across the subclusters. Among the most upregulated genes in PHGs were markers for beta cell dysfunction (*ALDOB*, *RBP4)* [50, 51]. Validation of RBP4, which marks beta cells with reduced functional capacity, reduced exocytosis, and altered stimulus-secretion coupling [50], revealed a pronounced increase in expression in the majority of beta cells in PHGs (Fig. 4h), indicating a global detrimental impact of maternal diabetes on offspring beta cell health.

In addition, two genes associated with cellular stress response (*DNAJB1*, *HSPA5*) [52] were among the top 15 upregulated genes in beta cells of PHGs, along with other markers of disrupted cellular homeostasis (*HMGB2, RHOB, B2M, IFI6, PCSK1N*) (Fig. 4g). Chronically elevated glucose levels have well-documented detrimental effects on beta cells, many of which were also evident in beta cells of PHGs. These included increased endoplasmic reticulum (ER) stress driven by activation of the unfolded protein response (UPR) [53]. In beta$^{rp\text{-}high}$ cells of PHGs, strong transcript upregulation of *PDIA6*, *ATF4* and *HSPA5* indicated activation of all three UPR pathways (Fig. 4i). In contrast, in the beta$^{rp\text{-}low}$ subcluster, the integrated stress response pathway PERK with *ATF4* upregulation was preferentially activated. Notably, nearly half of all detected immediate early genes, which constitute a first line of defence against cellular stress by initiating adaptive response mechanisms [54], were upregulated in beta cells of PHGs, most of them selectively in beta$^{rp\text{-}low}$ cells (ESM Fig. 9). The transcriptome signature (including *NPAS4* [53], which was among the top 15 upregulated genes in beta$^{rp\text{-}low}$ cells; the NPAS4 target gene *RGS2*, which attenuates the Gs-adenylyl cyclase signalling pathway [53]; *MCL1*, the product of which prevents beta cell death [55]; and *NR4A1*, which protects beta cells from oxidative stress-induced apoptosis [56]) suggests an adaptive, pro-survival transcriptional reactivity of beta$^{rp\text{-}low}$ cells in PHGs.

Molecular features of beta cell dysfunction in PHGs indicate altered glucose sensing and energy metabolism, compounded by disrupted calcium homeostasis To address the question of why the pancreas of PHGs exhibited permanently elevated insulin secretion that was, in contrast to the pancreas in PNGs, non-responsive to a glucose stimulus, three of the top 15 downregulated genes in PHG beta cells attracted our attention: *SLC2A2*, encoding the major glucose transporter GLUT2 [57]; *HADH*, encoding an enzyme involved in mitochondrial β-oxidation of medium- and short-chain fatty acids [58]; and *CALB1*, encoding the major cellular calcium buffer [59]. The first two genes are involved in the initiation of insulin secretion and in the induction of ATP synthesis in healthy beta cells that precedes insulin secretion. GLUT2 was only faintly detectable in a subset of beta cells from PHGs, in stark contrast to its strong membrane localisation in all beta cells from PNGs (Fig. 5a–c), indicating profound impairment of glucose uptake and sensing in PHG beta cells. In addition, transcript levels of further genes involved in glucose utilisation were altered in beta cells from PHGs, including increased *ALDOB*, a marker of dysfunctional beta cells [51], and *ALDOC*. Further, decreased levels of *G6PC2* mRNA, which encodes a negative regulator of basal GSIS [60], and increased *PFKFB3* expression were observed in a subset of beta cells from PHGs. PFKFB3 is responsible for the synthesis of fructose 2,6-bisphosphate, a key metabolite in the dynamic regulation of glycolytic flux [61]. Alterations in the metabolism of nutrients other than glucose and alterations in cellular ATP production may also contribute to beta cell dysfunction in PHGs. Supporting this notion, *HADH* transcripts, coding a key enzyme involved in the utilisation of NEFA for ATP generation [58], were markedly downregulated in nearly all PHG beta cells.

Due to these transcript alterations of genes involved in energy metabolism in beta cells, we next examined the expression profiles of 'disallowed' genes that are normally silenced in mature beta cells but are reactivated during dedifferentiation of beta cells. Transcripts of five out of 17 disallowed genes detected in pig beta cells were more abundant in at least one subcluster in PHGs: *HPGD*, coding an enzyme responsible for the breakdown of inflammatory prostaglandins; *SMOC2*, coding a secreted calcium-binding protein with unknown role in islets; *MGLL* and *ACOT7*, encoding enzymes involved in the hydrolysis of monoacyl glycerol and of long-chain-acyl-CoAs, respectively; and *CXCL12*, coding a chemokine involved in immune regulation [62].


a
Gi
Gs
Gq
GPCRs
Adenylyl cyclase
ATP
cAMP
PKA
PLCE1
PLCB1rp-high
PIP2
IP3
DAG
Ca2+
PKCα
Insulin release
Insulin granule
Aa Upregulated in PHG
PRKCA
PNG
PHG
b
DAPI/INS/PKCα
DAPI/PKCα
PNG
PHG
c
DAPI/INS/p-mTOR
p-mTOR
DAPI/INS
PNG
PHG
Single INSpositive p-mTORnegative cell in PHG pancreas
d
DAPI/p-RAPTOR
DAPI/INS
PNG
PHG
INSnegative p-RAPTORpositive cell
e
ATF4
PNG
PHG
Branched chain amino acid transport through membrane
SLC3A2rp-high
SLC7A8
RRAGDrp-low
CASTOR2rp-low
ATP
ADP
AMPK
PRKAB2
TSC1/TSC2
RHEB
mTORC1
EIF4EBP1
ATF4
EIF4G1rp-low
RPS6KB1
(= p70 S6K)
RPS6
EEF2K
Growth factors via growth factor receptor pathway
IRS2rp-low
PIK3CA/PIK3C3
/PIK3R2
PIK3IP1
YWHAH
AKT1/AKT2
AKT3
AKT1S1
mTORC2
PRKCA
AKT3
PNG
PHG
mRNA translation – metabolic homeostasis – protein turnover
Cytoskeleton rearrangement – cell migration
Aa Upregulated in PHG
Aa Downregulated in PHG
Inhibition
Activation
Activation by phosphorylation

◂**Fig. 6** Hallmarks of alterations in signalling pathways in beta cells from PHGs. (**a**) Schematic overview of the amplification pathway of insulin secretion mediated by GPCR downstream signalling, with UMAP plots for *PRKCA*. (**b**–**d**) Representative immunofluorescence confocal images of pancreas stained for insulin-PKCα (**b**), insulin-phospho-mTOR (Ser2448) (**c**) and insulin-phospho-RAPTOR (Ser792) (**d**). Animals' age: 3 days (**b**, **c**) or 2 days (**d**). Scale bar, 20 μm (**b**) or 50 μm (**c**, **d**). (**e**) Schematic representation of mTOR signalling, highlighting DEGs in beta cells from PHGs upstream and downstream of mTORC1 and mTORC2, with UMAP plots for *ATF4* and *AKT3*. INS, insulin

However, all of them were detected only in a small cell fraction (Fig. 5d).

For regulated insulin secretion, Ca^{2+} dynamics and currents are major determinants. Notably, the potent Ca^{2+}-buffering protein calbindin D28K, encoded by *CALB1*, was pronouncedly diminished in most of the beta cells from PHGs (Fig. 5e, f), which is suggestive of a disturbed Ca^{2+} buffering and, consequently, in Ca^{2+} homeostasis.

Altered mechanistic target of rapamycin and cAMP-responsive element binding protein signalling pathways in beta cells from PHGs Understanding the regulatory network underlying the beta cell dysfunction in PHGs was our next focus. The G-protein-coupled receptor (GPCR)–$G_{\alpha s}$-adenylyl cyclase-cAMP-protein kinase A (PKA) pathway is one of the key signalling cascades regulating glucose homeostasis and insulin secretion in healthy beta cells, along with mechanistic target of rapamycin (mTOR), a central regulator of nutrient sensing that is modulated by overnutrition [63–65]. Numerous transcriptional alterations in the GPCR regulatory network were observed, including *PRKCA*, which encodes protein kinase C (PKC) α (ESM Fig. 10). GPCR–$G_{\alpha q}$ downstream signalling via the second messengers diacylglycerol (DAG) and inositol 1,4,5-trisphosphate (IP3) might be activated in most beta cells of PHGs, as indicated by the marked increase of the DAG downstream target PKCα in the majority of these cells (Fig. 6a, b).

Focusing on the mTOR signalling, we first looked at phosphorylated RPS6, a downstream target of the mTORC1 complex that was reported to disappear in pancreatic beta cells in the course of the nutrient switch from suckling to carbohydrate-rich food [66]. Due to its similar staining pattern in PHGs and PNGs, with low staining intensity in most beta cells (ESM Fig. 11a), we next examined the mTOR complex itself. Phosphorylated mTOR (Ser2448) protein was markedly increased in most beta cells of the pancreas from neonatal PHGs, in contrast to PNGs (Fig. 6c), indicating strong mTOR pathway activation in the beta cells of PHGs. A similar staining pattern in beta cells from PHGs and PNGs was observed for the mTORC1 complex subunit RAPTOR, phosphorylated at Ser792 (Fig. 6d). Phosphorylation at Ser792 (i.e. the phosphorylation site at which the energy stress sensor AMPK mediates inhibition of mTORC1) leads to an inhibition of mTORC1 activity by RAPTOR [67]. We were unable to identify additional antibodies specific for components of mTORC complexes, upstream regulators or downstream targets working on porcine tissue. In our scRNA-seq data, we identified altered transcript levels of numerous genes of the mTOR signalling pathway; among them, the most robust upregulation was found for *ATF4*, a downstream target of mTORC1 (Fig. 6e and ESM Fig. 11b, c). In addition, transcript levels of the mTORC2 substrates AKT3 and PRKCA [68] were markedly increased, indicating an involvement of the mTORC2 pathway as well. Furthermore, the active form of the transcription factor cAMP-responsive element binding protein (CREB) was markedly increased in all beta cells from PHGs but was undetectable in those from PNGs (ESM Fig. 11d).

Discussion

As offspring of diabetic mothers are predisposed to developing type 2 diabetes later in life, insights into the functional and molecular changes of beta cells at birth are essential. Exposure to maternal hyperglycaemia induces fetal hyperinsulinaemia already in utero. In contrast, in offspring of normoglycaemic mothers, pancreatic beta cells are responsive to amino acid-stimulated insulin secretion but not GSIS during the fetal period, acquiring glucose sensitivity only after birth [69]. Due to the limited availability of human neonatal pancreatic tissue, current knowledge of the functional and molecular alterations of beta cells from offspring of diabetic mothers is incomplete. In our study, we identified distinct functional, structural and molecular consequences of maternal diabetes on fetal pancreatic development.

Similar to what is observed in humans [7], the PHGs, born to hyperglycaemic mothers, exhibited fetal hyperglycaemia and hyperinsulinaemia in response to chronically elevated placental glucose transfer and, consequently, developed insulin resistance. In humans, offsprings' serum insulin levels depend more on the duration than on the degree of fetal hyperglycaemia [70]. Notably, the molecular profile of beta cells from neonatal PHGs closely resembles, at first glance, the profiles of beta cells of type 2 diabetes in humans. For instance, increased *ALDOB* and decreased *GLUT2* expression showed the strongest associations with HbA_{1c} levels in type 2 diabetes, suggesting progressive changes as glucose regulation deteriorates [51, 71]. However, in contrast to type 2 diabetes, where dysfunctional beta cells arise through dedifferentiation or dysregulation from mature beta cells, loss of beta cell identity and expression of disallowed genes [50, 57, 71], the type 2 diabetes-like

phenotype of dysfunctional beta cells in PHGs may have a different origin. There, endocrine cells in the fetal pancreas are negatively affected by chronic hyperglycaemia during the sensitive period of pancreatic organogenesis and growth. This period of highest plasticity [1] is characterised by differentiation, maturation and morphological rearrangements of endocrine cells that lead to the formation of the islets of Langerhans.

In our study, the marked increase in endocrine cell content and accelerated clustering into islets in PHGs initially suggested accelerated maturation. These findings would align with the hypothesis of accelerated fetal islet and beta cell maturation previously proposed for offspring of diabetic mothers, based on findings of sustained fetal hyperinsulinism and rapid early insulin responses in islet-like clusters from mid-gestation human fetuses [72]. Similarly, a rodent study of a maternal low-protein diet in small-for-gestational-age offspring proposed early beta cell maturation resulting from a premature switch from proliferation to differentiation during the perinatal period [73]. However, the structural alterations observed in our pig study, including increased beta cell content and accelerated cluster formation in the pancreas of PHGs, were not accompanied by a more mature transcriptome signature than in PNGs, nor by functional maturation with a glucose-regulated insulin secretion. Instead, beta cells in PHGs were dysfunctional, with altered transcript and protein profiles of genes involved at multiple levels in beta cell function. GSIS in PHGs was markedly altered, with pronounced basal insulin hypersecretion and a near-blunted first-phase insulin secretion. Initiation of insulin secretion by glucose uptake might already be compromised by a markedly reduced GLUT2 transporter protein abundance. Among the various alterations affecting energy metabolism, the pronounced downregulation of *HADH* transcripts may contribute to the marked basal hypersecretion of insulin observed in beta cells of neonatal PHGs. This interpretation is consistent with findings in humans carrying loss-of-function mutations in *HADH*, which cause congenital hyperinsulinism [58].

Additional components of the complex machinery coordinating insulin secretion may also be impaired in dysfunctional beta cells of PHGs. For example, calbindin D28K modulates GSIS through multiple mechanisms, including regulation of L-type voltage-gated Ca^{2+} channels and the resulting Ca^{2+} influx, as well as intracellular Ca^{2+} buffering. Increased expression of calbindin D28K has been reported to suppress GSIS [74, 75]. However, despite the near absence of calbindin D28K, GSIS was markedly diminished in beta cells of PHGs. Further, the GPCR ligands that may have driven the predominance of the GPCR–Gαq–PLC–DAG–PKCα pathway in insulin secretion amplification remain unidentified. Similar uncertainties apply to alterations in mTOR signalling in beta cells of PHGs. Phosphorylation of mTOR at Ser2448, together with activation of its downstream targets S6K1 and RPS6, is generally considered indicative of mTORC1 activation (reviewed in [76]); however, our findings are not consistent with this interpretation. Notably, mTORC1 signalling extends beyond the regulation of protein translation, and mTOR phosphorylated at Ser2448 has also been detected within the mTORC2 complex [77]. Moreover, elucidating the roles of both mTORC1 and the less extensively studied mTORC2 in diabetes remains an active area of investigation [64]. The duration of metabolic stress may represent an additional determinant, as a switch from $G_{\alpha s}$- to $G_{\alpha q}$-mediated signalling has been identified as an adaptive mechanism in beta cells exposed to chronic hyperglycaemia [78]. One potential contributor to the complex alterations observed in beta cells of PHGs is the robust global transcriptional upregulation of components of the PERK–ATF4 arm of the UPR. Another notable finding was the widespread presence of active CREB1 in beta cells of PHGs. Because CREB1 can be activated not only through the GPCR–Gαs–adenylyl cyclase–cAMP–PKA pathway but also via other signalling pathways, including Ca^{2+}-dependent and stress-related signalling [79], both of which were altered in beta cells of PHGs, and because CREB1 regulates a broad repertoire of target genes, the mechanistic consequences of its activation in PHG beta cells remain unclear. A limitation of the present study is that the single postnatal time point precludes identification of the developmental processes underlying endocrine cell dysfunction. Establishing causality will require longitudinal in vivo studies with gestational interventions.

In conclusion, using a clinically relevant pig model, our study provides a comprehensive characterisation of the structural and molecular alterations associated with beta cell dysfunction in neonatal offspring of diabetic mothers, thereby extending current understanding of the early effects of maternal diabetes on the endocrine pancreas. Given the similarities in beta cell development between pigs and humans [10], our findings are likely to be relevant to offspring born to mothers with preconceptional and possibly also gestational diabetes.

Supplementary Information The online version of this article (https://doi.org/10.1007/s00125-026-06906-z) contains peer-reviewed but unedited supplementary material.

Acknowledgements We would like to thank all members of the CiMM for their excellent animal care and support. Our thanks also go to C. Blechinger, A. Shabani, F. Stotz and T. Schröter from the Chair for Molecular Animal Breeding and Biotechnology for their outstanding technical support. The authors would like to express their gratitude to the Core Facility Pathology & Tissue Analytics at the Helmholtz Center Munich for their contribution to creating WSIs, as well as for granting access to the imaging facility at the Gene Center, LMU Munich. Sequencing was performed at the Helmholtz Zentrum München by the Genomics Core Facility. Figures were created with BioRender.com, where indicated. Grammarly was used for language

grammar correction. Parts of the manuscript's findings were used for the PhD thesis of the manuscript's first author Libera Valla at the Chair for Molecular Animal Breeding and Biotechnology of LMU Munich.

Data and code availability Raw and processed sequencing data will be available upon publication of the research article. Proteomics data generated in this study are available on the PRIDE repository (ProteomeXchange) under the accession number PXD071507. scRNA-seq data from this study have been deposited in the Gene Expression Omnibus (GEO) under accession number GSE316579 and are publicly available at https://www.ncbi.nlm.nih.gov/geo/query/acc.cgi?acc=GSE316579. Requests for further information and resources should be directed to and will be fulfilled by the corresponding author.

Funding Open Access funding enabled and organized by Projekt DEAL. This project received funding from the European Union's Horizon 2020 research and innovation programme under the Marie Skłodowska-Curie grant agreement no. 812660 (DohART-NET to EW and TF); from the Deutsche Forschungsgemeinschaft (TRR205 [to EK and EW], project no. 458958943 [to EW, HL and FJT; in association with DFG Research Infrastructure NGS_CC, project 407495230, as part of the Next Generation Sequencing Competence Network, project 423957469 – for scRNA-seq], project no. 534046536 [to TF for MS instrumentation]), from Breakthrough T1D (formerly known as JDRF; grant no. 3-SRA-2023-1420-S-B to EW, HL), and from the German Federal Ministry of Education and Research (BMBF) to the German Centre for Diabetes Research (grant no. 82DZD00802 to EW).

Authors' relationships and activities FJT consults for Immunai, CytoReason, Genbio and Valinor Industries, and has ownership interest in RN.AI Therapeutics, Dermagnostix and Cellarity. All other authors declare that there are no relationships or activities that might bias, or be perceived to bias, their work.

Contribution statement EW and EK conceived the study. MFS, JBS, MS and TF curated the data. Formal analyses were performed by LV, MFS, CMC, JBS, CK, BR, AB, TF, EW and EK. Investigations were carried out by LV, MFS, CMC, JBS, CK, BS, BR, RL, MK, SR, MMvdB, KY, MS, AB, TF and EK. Methodology was developed by CMC, BS, MHdA, MS, SS, TF, FJT and HL. Resources were provided by MHdA, SS, TF, HL and EW and software was developed by FJT. Data visualisation was undertaken by MFS, CMC, JBS and EK. Funding was acquired by TF, FJT, HL, EW and EK. LV and EK wrote the original draft of the manuscript. All authors reviewed the manuscript critically for important intellectual content and contributed to its revision. All authors approved the final version of the manuscript and agree to be accountable for all aspects of the work. EK is the guarantor of this work.

Open Access This article is licensed under a Creative Commons Attribution 4.0 International License, which permits use, sharing, adaptation, distribution and reproduction in any medium or format, as long as you give appropriate credit to the original author(s) and the source, provide a link to the Creative Commons licence, and indicate if changes were made. The images or other third party material in this article are included in the article's Creative Commons licence, unless indicated otherwise in a credit line to the material. If material is not included in the article's Creative Commons licence and your intended use is not permitted by statutory regulation or exceeds the permitted use, you will need to obtain permission directly from the copyright holder. To view a copy of this licence, visit http://creativecommons.org/licenses/by/4.0/.

References

1. Jo S, Alejandro EU (2023) RISING STARS: Mechanistic insights into maternal-fetal cross talk and islet beta-cell development. J Endocrinol 259(3):e230069. https://doi.org/10.1530/JOE-23-0069
2. Lowe WL Jr, Scholtens DM, Kuang A et al (2019) Hyperglycemia and Adverse Pregnancy Outcome Follow-up Study (HAPO FUS): maternal gestational diabetes mellitus and childhood glucose metabolism. Diabetes Care 42(3):372–380. https://doi.org/10.2337/dc18-1646
3. Shashikadze B, Flenkenthaler F, Stockl JB et al (2021) Developmental effects of (Pre-)Gestational diabetes on offspring: systematic screening using omics approaches. Genes (Basel) 12(12):1991. https://doi.org/10.3390/genes12121991
4. Clausen TD, Mathiesen ER, Hansen T et al (2008) High prevalence of type 2 diabetes and pre-diabetes in adult offspring of women with gestational diabetes mellitus or type 1 diabetes: the role of intrauterine hyperglycemia. Diabetes Care 31(2):340–346. https://doi.org/10.2337/dc07-1596
5. Pedersen J (1952) Diabetes and pregnancy; blood sugar of newborn infants during fasting and glucose administration. Ugeskr Laeger 114(21):685
6. Herrera E, Ortega-Senovilla H (2018) Implications of lipids in neonatal body weight and fat mass in gestational diabetic mothers and non-diabetic controls. Curr Diab Rep 18(2):7. https://doi.org/10.1007/s11892-018-0978-4
7. Rajamoorthi A, Zheng H, Skowronski AA et al (2025) Association of gestational and childhood circulating C-peptide concentrations in the hyperglycemia and adverse pregnancy outcomes follow-up study. Diabetes Res Clin Pract 220:111967. https://doi.org/10.1016/j.diabres.2024.111967
8. Barker DJP (2012) Sir Richard Doll Lecture. Developmental origins of chronic disease. Public Health 126(3):185–189. https://doi.org/10.1016/j.puhe.2011.11.014
9. Hoffman DJ, Powell TL, Barrett ES, Hardy DB (2021) Developmental origins of metabolic diseases. Physiol Rev 101(3):739–795. https://doi.org/10.1152/physrev.00002.2020
10. Yang K, Spitzer H, Sterr M et al (2025) A multimodal cross-species comparison of pancreas development. Nat Commun 16(1):9355. https://doi.org/10.1038/s41467-025-64774-4
11. Renner S, Braun-Reichhart C, Blutke A et al (2013) Permanent neonatal diabetes in INS(C94Y) transgenic pigs. Diabetes 62(5):1505–1511. https://doi.org/10.2337/db12-1065
12. Kemter E, Cohrs CM, Schafer M et al (2017) INS-eGFP transgenic pigs: a novel reporter system for studying maturation, growth and vascularisation of neonatal islet-like cell clusters. Diabetologia 60(6):1152–1156. https://doi.org/10.1007/s00125-017-4250-2
13. Renner S, Martins AS, Streckel E et al (2019) Mild maternal hyperglycemia in INS^{C93S} transgenic pigs causes impaired glucose tolerance and metabolic alterations in neonatal offspring. Dis Model Mech 12(8):dmm039156. https://doi.org/10.1242/dmm.039156
14. Eckstein Y, Kessler B, Hinrichs A et al (2025) Protocol for in vivo assessment of glucose control and insulin secretion and sensitivity in the pig. STAR Protoc 6(2):103774. https://doi.org/10.1016/j.xpro.2025.103774
15. Shashikadze B, Valla L, Lombardo SD et al (2023) Maternal hyperglycemia induces alterations in hepatic amino acid, glucose and lipid metabolism of neonatal offspring: Multi-omics insights from a diabetic pig model. Mol Metab 75:101768. https://doi.org/10.1016/j.molmet.2023.101768

16. Matsuda M, DeFronzo RA (1999) Insulin sensitivity indices obtained from oral glucose tolerance testing: comparison with the euglycemic insulin clamp. Diabetes Care 22(9):1462–1470. https://doi.org/10.2337/diacare.22.9.1462
17. Katz A, Nambi SS, Mather K et al (2000) Quantitative insulin sensitivity check index: a simple, accurate method for assessing insulin sensitivity in humans. J Clin Endocrinol Metab 85(7):2402–2410. https://doi.org/10.1210/jcem.85.7.6661
18. Dietrich JW, Dasgupta R, Anoop S et al (2022) SPINA Carb: a simple mathematical model supporting fast in-vivo estimation of insulin sensitivity and beta cell function. Sci Rep 12(1):17659. https://doi.org/10.1038/s41598-022-22531-3
19. Dietrich JW, Abood A, Dasgupta R et al (2024) A novel simple disposition index (SPINA-DI) from fasting insulin and glucose concentration as a robust measure of carbohydrate homeostasis. J Diabetes 16(9):e13525. https://doi.org/10.1111/1753-0407.13525
20. Albl B, Haesner S, Braun-Reichhart C et al (2016) Tissue sampling guides for porcine biomedical models. Toxicol Pathol 44(3):414–420. https://doi.org/10.1177/0192623316631023
21. Marciniak A, Cohrs CM, Tsata V et al (2014) Using pancreas tissue slices for in situ studies of islet of Langerhans and acinar cell biology. Nat Protoc 9(12):2809–2822. https://doi.org/10.1038/nprot.2014.195
22. Demichev V, Messner CB, Vernardis SI, Lilley KS, Ralser M (2020) DIA-NN: neural networks and interference correction enable deep proteome coverage in high throughput. Nat Methods 17(1):41–44. https://doi.org/10.1038/s41592-019-0638-x
23. R Core Team (2021) R: A language and environment for statistical computing [Computer software]
24. Tyanova S, Temu T, Sinitcyn P et al (2016) The Perseus computational platform for comprehensive analysis of (prote)omics data. Nat Methods 13(9):731–740. https://doi.org/10.1038/nmeth.3901
25. Tusher VG, Tibshirani R, Chu G (2001) Significance analysis of microarrays applied to the ionizing radiation response. Proc Natl Acad Sci U S A 98(9):5116–5121. https://doi.org/10.1073/pnas.091062498
26. Perez-Riverol Y, Bai J, Bandla C et al (2022) The PRIDE database resources in 2022: a hub for mass spectrometry-based proteomics evidences. Nucleic Acids Res 50(D1):D543–D552. https://doi.org/10.1093/nar/gkab1038
27. Kemter E, Muller A, Neukam M et al (2021) Sequential in vivo labeling of insulin secretory granule pools in INS-SNAP transgenic pigs. Proc Natl Acad Sci U S A 118(37):e2107665118. https://doi.org/10.1073/pnas.2107665118
28. Wolf FA, Angerer P, Theis FJ (2018) SCANPY: large-scale single-cell gene expression data analysis. Genome Biol 19(1):15. https://doi.org/10.1186/s13059-017-1382-0
29. Lun ATL, Riesenfeld S, Andrews T et al (2019) EmptyDrops: distinguishing cells from empty droplets in droplet-based single-cell RNA sequencing data. Genome Biol 20(1):63. https://doi.org/10.1186/s13059-019-1662-y
30. Luecken MD, Theis FJ (2019) Current best practices in single-cell RNA-seq analysis: a tutorial. Mol Syst Biol 15(6):e8746. https://doi.org/10.15252/msb.20188746
31. Wolock SL, Lopez R, Klein AM (2019) Scrublet: computational identification of cell doublets in single-cell transcriptomic data. Cell Syst 8(4):281–291.e289. https://doi.org/10.1016/j.cels.2018.11.005
32. Gayoso A, Shor J, Carr AJ, R. S, D. Pe (2019) GitHub: DoubletDetection (v2.4.1). In: Zenodo (software)
33. Germain PL, Lun A, Garcia Meixide C, Macnair W, Robinson MD (2021) Doublet identification in single-cell sequencing data using scDblFinder. F1000Res 10:979. https://doi.org/10.12688/f1000research.73600.2
34. Bais AS, Kostka D (2020) scds: computational annotation of doublets in single-cell RNA sequencing data. Bioinformatics 36(4):1150–1158. https://doi.org/10.1093/bioinformatics/btz698
35. McGinnis CS, Murrow LM, Gartner ZJ (2019) DoubletFinder: doublet detection in single-cell RNA sequencing data using artificial nearest neighbors. Cell Syst 8(4):329-337 e324. https://doi.org/10.1016/j.cels.2019.03.003
36. Lun AT, Bach K, Marioni JC (2016) Pooling across cells to normalize single-cell RNA sequencing data with many zero counts. Genome Biol 17:75. https://doi.org/10.1186/s13059-016-0947-7
37. Gayoso A, Lopez R, Xing G et al (2022) A Python library for probabilistic analysis of single-cell omics data. Nat Biotechnol 40(2):163–166. https://doi.org/10.1038/s41587-021-01206-w
38. Becht E, McInnes L, Healy J et al (2019) Dimensionality reduction for visualizing single-cell data using UMAP. Nat Biotechnol 37:38–44. https://doi.org/10.1038/nbt.4314
39. Zappia L, Oshlack A (2018) Clustering trees: a visualization for evaluating clusterings at multiple resolutions. Gigascience 7(7):giy083. https://doi.org/10.1093/gigascience/giy083
40. Satija R, Farrell JA, Gennert D, Schier AF, Regev A (2015) Spatial reconstruction of single-cell gene expression data. Nat Biotechnol 33(5):495–502. https://doi.org/10.1038/nbt.3192
41. Hafemeister C (2026) GitHub: DElegate (v1.2.1) [software]. https://github.com/cancerbits/DElegate
42. Chen Y, Chen L, Lun ATL, Baldoni PL, Smyth GK (2025) edgeR v4: powerful differential analysis of sequencing data with expanded functionality and improved support for small counts and larger datasets. Nucleic Acids Res 53(2):gkaf018. https://doi.org/10.1093/nar/gkaf018
43. Bankhead P, Loughrey MB, Fernandez JA et al (2017) QuPath: open source software for digital pathology image analysis. Sci Rep 7(1):16878. https://doi.org/10.1038/s41598-017-17204-5
44. Apaolaza PS, Petropoulou PI, Rodriguez-Calvo T (2021) Whole-slide image analysis of human pancreas samples to elucidate the immunopathogenesis of type 1 diabetes using the QuPath software. Front Mol Biosci 8:689799. https://doi.org/10.3389/fmolb.2021.689799
45. Ahlqvist E, Storm P, Karajamaki A et al (2018) Novel subgroups of adult-onset diabetes and their association with outcomes: a data-driven cluster analysis of six variables. Lancet Diabetes Endocrinol 6(5):361–369. https://doi.org/10.1016/S2213-8587(18)30051-2
46. Pantham P, Aye IL, Powell TL (2015) Inflammation in maternal obesity and gestational diabetes mellitus. Placenta 36(7):709–715. https://doi.org/10.1016/j.placenta.2015.04.006
47. Dorrell C, Schug J, Canaday PS et al (2016) Human islets contain four distinct subtypes of beta cells. Nat Commun 7:11756. https://doi.org/10.1038/ncomms11756
48. Walker JT, Saunders DC, Rai V et al (2023) Genetic risk converges on regulatory networks mediating early type 2 diabetes. Nature 624(7992):621–629. https://doi.org/10.1038/s41586-023-06693-2
49. Brown ME, Miranda VE, Nevills S et al (2025) Pancreatic islet beta-cell subtypes are derived from biochemically-distinct and nutritionally-regulated islet progenitors. Nat Commun 16(1):5758. https://doi.org/10.1038/s41467-025-60831-0
50. Camunas-Soler J, Dai XQ, Hang Y et al (2020) Patch-Seq links single-cell transcriptomes to human islet dysfunction in diabetes. Cell Metab 31(5):1017–1031.e1014. https://doi.org/10.1016/j.cmet.2020.04.005
51. Wigger L, Barovic M, Brunner AD et al (2021) Multi-omics profiling of living human pancreatic islet donors reveals heterogeneous beta cell trajectories towards type 2 diabetes. Nat Metab 3(7):1017–1031. https://doi.org/10.1038/s42255-021-00420-9
52. Maestas MM, Ishahak M, Augsornworawat P et al (2024) Identification of unique cell type responses in pancreatic islets to stress. Nat Commun 15(1):5567. https://doi.org/10.1038/s41467-024-49724-w

53. Sabatini PV, Krentz NA, Zarrouki B et al (2013) Npas4 is a novel activity-regulated cytoprotective factor in pancreatic beta-cells. Diabetes 62(8):2808–2820. https://doi.org/10.2337/db12-1527
54. Fowler T, Sen R, Roy AL (2011) Regulation of primary response genes. Mol Cell 44(3):348–360. https://doi.org/10.1016/j.molcel.2011.09.014
55. Meyerovich K, Violato NM, Fukaya M et al (2017) MCL-1 Is a key antiapoptotic protein in human and rodent pancreatic beta-cells. Diabetes 66(9):2446–2458. https://doi.org/10.2337/db16-1252
56. Zong C, Qin D, Yu C et al (2017) The stress-response molecule NR4A1 resists ROS-induced pancreatic beta-cells apoptosis via WT1. Cell Signal 35:129–139. https://doi.org/10.1016/j.cellsig.2017.03.012
57. Hrovatin K, Bastidas-Ponce A, Bakhti M et al (2023) Delineating mouse beta-cell identity during lifetime and in diabetes with a single cell atlas. Nat Metab 5(9):1615–1637. https://doi.org/10.1038/s42255-023-00876-x
58. St-Louis JL, El Jellas K, Velasco K et al (2023) Deficiency of the metabolic enzyme SCHAD in pancreatic beta-cells promotes amino acid-sensitive hypoglycemia. J Biol Chem 299(8):104986. https://doi.org/10.1016/j.jbc.2023.104986
59. Pujol JB, Heikkila E, Savoia C et al (2018) Isx9 regulates calbindin D28K expression in pancreatic beta cells and promotes beta cell survival and function. Int J Mol Sci 19(9):2542. https://doi.org/10.3390/ijms19092542
60. Pound LD, Oeser JK, O'Brien TP et al (2013) G6PC2: a negative regulator of basal glucose-stimulated insulin secretion. Diabetes 62(5):1547–1556. https://doi.org/10.2337/db12-1067
61. Raval K, Jamshidi N, Seyran B et al (2024) Dysfunctional beta-cell longevity in diabetes relies on energy conservation and positive epistasis. Life Sci Alliance 7(12):e202402743. https://doi.org/10.26508/lsa.202402743
62. Rutter GA, Georgiadou E, Martinez-Sanchez A, Pullen TJ (2020) Metabolic and functional specialisations of the pancreatic beta cell: gene disallowance, mitochondrial metabolism and intercellular connectivity. Diabetologia 63(10):1990–1998. https://doi.org/10.1007/s00125-020-05205-5
63. Yang H, Yang L (2016) Targeting cAMP/PKA pathway for glycemic control and type 2 diabetes therapy. J Mol Endocrinol 57(2):R93–R108. https://doi.org/10.1530/JME-15-0316
64. Ardestani A, Lupse B, Kido Y, Leibowitz G, Maedler K (2018) mTORC1 signaling: a double-edged sword in diabetic beta cells. Cell Metab 27(2):314–331. https://doi.org/10.1016/j.cmet.2017.11.004
65. Xu P (2025) mTORC1 is the central regulator in pancreatic beta-cells. Nat Rev Endocrinol 21(6):330. https://doi.org/10.1038/s41574-025-01116-w
66. Jaafar R, Tran S, Shah AN et al (2019) mTORC1 to AMPK switching underlies beta-cell metabolic plasticity during maturation and diabetes. J Clin Invest 129(10):4124–4137. https://doi.org/10.1172/JCI127021
67. Gwinn DM, Shackelford DB, Egan DF et al (2008) AMPK phosphorylation of raptor mediates a metabolic checkpoint. Mol Cell 30(2):214–226. https://doi.org/10.1016/j.molcel.2008.03.003
68. Ragupathi A, Kim C, Jacinto E (2024) The mTORC2 signaling network: targets and cross-talks. Biochem J 481(2):45–91. https://doi.org/10.1042/BCJ20220325
69. Helman A, Cangelosi AL, Davis JC et al (2020) A nutrient-sensing transition at birth triggers glucose-responsive insulin secretion. Cell Metab 31(5):1004-1016 e1005. https://doi.org/10.1016/j.cmet.2020.04.004
70. Grasso S, Palumbo G, Messina A, Mazzarino C, Reitano G (1976) Human maternal and fetal serum insulin and growth hormone (HGH) response to glucose and leucine. Diabetes 25(7):545–549. https://doi.org/10.2337/diab.25.7.545
71. Wang G, Sander M (2021) A multi-omics roadmap of beta-cell failure in type 2 diabetes mellitus. Nat Rev Endocrinol 17(11):641–642. https://doi.org/10.1038/s41574-021-00556-4
72. Otonkoski T, Andersson S, Knip M, Simell O (1988) Maturation of insulin response to glucose during human fetal and neonatal development. Studies with perifusion of pancreatic isletlike cell clusters. Diabetes 37(3):286–291. https://doi.org/10.2337/diab.37.3.286
73. Rodriguez-Trejo A, Ortiz-Lopez MG, Zambrano E et al (2012) Developmental programming of neonatal pancreatic beta-cells by a maternal low-protein diet in rats involves a switch from proliferation to differentiation. Am J Physiol Endocrinol Metab 302(11):E1431-1439. https://doi.org/10.1152/ajpendo.00619.2011
74. Sooy K, Schermerhorn T, Noda M et al (1999) Calbindin-D(28k) controls [Ca(2+)](i) and insulin release. Evidence obtained from calbindin-d(28k) knockout mice and beta cell lines. J Biol Chem 274(48):34343–34349. https://doi.org/10.1074/jbc.274.48.34343
75. Christensen GL, Jacobsen ML, Wendt A et al (2015) Bone morphogenetic protein 4 inhibits insulin secretion from rodent beta cells through regulation of calbindin1 expression and reduced voltage-dependent calcium currents. Diabetologia 58(6):1282–1290. https://doi.org/10.1007/s00125-015-3568-x
76. Szwed A, Kim E, Jacinto E (2021) Regulation and metabolic functions of mTORC1 and mTORC2. Physiol Rev 101(3):1371–1426. https://doi.org/10.1152/physrev.00026.2020
77. Rosner M, Siegel N, Valli A, Fuchs C, Hengstschlager M (2010) mTOR phosphorylated at S2448 binds to raptor and rictor. Amino Acids 38(1):223–228. https://doi.org/10.1007/s00726-008-0230-7
78. Oduori OS, Murao N, Shimomura K et al (2020) Gs/Gq signaling switch in beta cells defines incretin effectiveness in diabetes. J Clin Invest 130(12):6639–6655. https://doi.org/10.1172/JCI140046
79. Sabatini PV, Speckmann T, Lynn FC (2019) Friend and foe: beta-cell Ca(2+) signaling and the development of diabetes. Mol Metab 21:1–12. https://doi.org/10.1016/j.molmet.2018.12.007

Publisher's Note Springer Nature remains neutral with regard to jurisdictional claims in published maps and institutional affiliations.

Authors and Affiliations

Libera Valla[1,2] · Minas F. Schwager[3,4] · Christian M. Cohrs[5,6,7] · Jan B. Stoeckl[8] · Christos Karampelias[3,5] · Bachuki Shashikadze[8] · Birgit Rathkolb[1,5,9] · Richard Lindner[1,2] · Martin Kraetzl[1,2] · Simone Renner[1,2,5,10] · Mireia Molina van den Bosch[3] · Kaiyuan Yang[3] · Michael Sterr[3,5] · Anika Böttcher[3,5] · Martin Hrabě de Angelis[5,9,11] · Stephan Speier[5,6,7] · Thomas Fröhlich[8] · Fabian J. Theis[4] · Heiko Lickert[3,5] · Eckhard Wolf[1,2,5,8,10] · Elisabeth Kemter[1,2,5,10]

✉ Elisabeth Kemter
E.Kemter@lmu.de

1 Chair for Molecular Animal Breeding and Biotechnology, Gene Center and Department of Veterinary Sciences, LMU Munich, Munich, Germany

2 Center for Innovative Medical Models (CiMM), LMU Munich, Oberschleissheim, Germany

3 Institute of Diabetes and Regeneration Research, Helmholtz Munich, Neuherberg, Germany

4 Institute of Computational Biology, Helmholtz Munich, Neuherberg, Germany

5 German Center for Diabetes Research (DZD), Neuherberg, Germany

6 Institute of Physiology, Faculty of Medicine, Technische Universität Dresden, Dresden, Germany

7 Paul Langerhans Institute Dresden (PLID) of the Helmholtz Zentrum München at the University Clinic Carl Gustav Carus of Technische Universität Dresden, Helmholtz Zentrum München, Neuherberg, Germany

8 Laboratory for Functional Genome Analysis (LAFUGA), Gene Center, LMU Munich, Munich, Germany

9 Institute of Experimental Genetics, German Mouse Clinic, Helmholtz Munich, Neuherberg, Germany

10 Interfaculty Center for Endocrine and Cardiovascular Disease Network Modelling and Clinical Transfer (ICONLMU), LMU Munich, Munich, Germany

11 Chair of Experimental Genetics, TUM School of Life Sciences, Technische Universität München, Freising, Germany